SUPPORTING INFORMATION

A Price to Pay for Relaxed Substrate Specificity: A Comparative Kinetic Analysis of the Class II Lanthipeptide Synthetases ProcM and HalM2

Christopher J. Thibodeaux,[1] Taekjip Ha,[1,2] and Wilfred A. van der Donk[1,3,*]

[1]Institute for Genomic Biology, [2]Department of Physics, [3]Department of Chemistry
University of Illinois, Urbana-Champaign
600 S. Mathews Ave, Urbana, IL. 61801
*email: vddonk@illinois.edu

I. General Methods

General: Reagents were purchased from Fisher (NaCl, $MgCl_2$, NaOH, Tris, and HEPES), Thermo Scientific (TCEP, formic acid), Sigma-Aldrich (ATP, sodium citrate, Trolox), J. T. Baker (EDTA), Alfa Aesar (imidazole, TFA), or Macron Fine Chemicals (glycerol, MeCN). Oligonucleotide primers were purchased from IDT. Unless otherwise noted, restriction enzymes and other reagents needed for molecular cloning were purchased from New England Biolabs. Raw kinetic data were processed with Excel (Microsoft) and OriginPro 9.1 (OriginLab Corporation). Numerical simulations of the kinetic data were performed with KinTek Explorer.[1,2] HiTrap columns for Ni-NTA affinity chromatography were purchased from GE Healthcare. HPLC was performed on a Shimadzu Prominence Preparative Liquid Chromatography system. MALDI-TOF MS was performed on a Voyager-DE instrument (Applied Biosciences). All plasmid constructs used in this study were sequenced by the Keck Center at the University of Illinois, Urbana-Champaign.

Preparation of LanA peptides: The wild type *procA2.8* and *halA2* genes from *Prochlorococcus* MIT9313 and *Bacillus halodurans*, respectively, were cloned into the NdeI/XhoI sites of pET15b as described previously.[3,4] Additionally, the three codons at the 5' end of the *halA2*/pET15 construct (coding for GlySerSer) were mutagenized to a single Pro codon by GenScript in order to minimize gluconylation of the His_6 tag during expression in *E. coli*.[5] The resulting clone was dubbed *his$_6$P-halA2*/*pET15b*. *E. coli* BL21 (DE3) cells were transformed with the vectors and the recombinant *N*-terminally His_6-tagged peptides were expressed and purified from 2 L of Luria broth (LB) culture by immobilized metal affinity chromatography (IMAC) as described previously.[6] Peptides were then desalted on Vydac 1 mL C4 solid phase extraction (C4-SPE) columns by loading 1 mL of the IMAC eluate, washing with 3 mL of 0.1% trifluoroacetic acid (TFA) in H_2O, then eluting with 2 mL of 0.1% TFA in 80% acetonitrile (MeCN). Crude peptides were flash frozen in liquid nitrogen, lyophilized,

redissolved in H_2O and stored at -20 °C until use. The His_6-affinity tag of His_6-ProcA2.8 was then removed by treatment with 50 units of high purity grade bovine thrombin (MP Biomedicals) in 25 mM potassium phosphate buffer (pH 7.0) at 4 °C for 24 h – leaving a GlySerHis tripeptide appended to the *N*-terminal end of the otherwise wild type ProcA2.8 sequence.[3] Thrombin digestion was not performed on the His_6P-HalA2 peptide prior to kinetic analysis because we consistently observed a partial, adventitious thrombin cleavage reaction within the HalA2 leader peptide that would have made quantitation of the peptide fractional abundances difficult (Figure S1). Peptides (ProcA2.8 and His_6P-HalA2) were purified by reversed phase HPLC using a Phenomenex Luna C5 semiprep column (250x10 mm, 10µ, 100 Å) at a flow rate of 7 mL/min and a gradient of 2 – 100% solvent B (80% MeCN in H_2O, 0.1% TFA) over 40 min (solvent A was 0.1% TFA in H_2O). Finally, peptides were lyophilized and stored as powder or in aqueous solution at -20 °C until use.

Preparation of LanM synthetases: The *procM* and *halM2* genes were cloned into pET28 as described previously.[3,4] The plasmids were used to transform *E. coli* BL21 (DE3), and the proteins were expressed as His_6-fusion proteins. LB cultures inoculated 1:100 with an overnight culture were grown at 37 °C until the OD_{600} = 0.4, at which point 0.25 mM isopropyl-β-D-1-thiogalactopyranoside (IPTG) was added to induce protein expression. The temperature of the culture was then reduced to 18 °C and the cultures were grown over night. Cells were harvested by centrifugation (8000 x *g*, 10 min, 4 °C), lysed by sonication in lysis buffer (25 mM Tris, 500 mM NaCl, 20 mM imidazole, 10% glycerol, pH 8.0), and centrifuged at 14,000 x *g* for 30 min at 4 °C. The supernatant was loaded onto a 5 mL Hi-Trap Ni-NTA affinity column, washed with 100 mL of lysis buffer, then eluted with 15 mL of elution buffer (same as lysis buffer except the concentration of imidazole was increased to 200 mM). The 15 mL sample was concentrated to approximately 3 mL using an Amicon Ultra Centrifugal Filter device with a 50 kDa MW cutoff (Millipore). The entire 3 mL sample was then purified by gel filtration chromatography (Superdex 200, 1.5 x 60 cm, GE Healthcare) using a 1 mL/min flow rate and an isocratic elution with 25 mM Tris, 500 mM NaCl, 10% glycerol, pH 8.0. Both proteins eluted in 3 peaks (aggregate, then oligomer, followed by monomer). The monomer fraction was collected, concentrated with a second Amicon centrifugal filtration (50 kDa), aliquoted into portions for one-time use, flash frozen in liquid nitrogen, and stored at -80 °C.

LanM inactivation assays. We verified that the quench conditions used for our kinetic assays were sufficient to eliminate LanM activity. LanM enzymes in storage buffer (25 mM Tris, 500 mM NaCl, 10% glycerol, pH 8.0) were diluted to a 10 µM final concentration in 100 µL of 100 mM citrate (pH 3.3) and were incubated for 10 min at 25 °C (very similar to the standard quench conditions). The pH of these mixtures was measured to be ~ 3.5 for each sample. These quenched enzyme samples were then diluted 10x into a standard 100 µL LanM/LanA reaction mixture at neutral pH (see Methods section in main text for conditions). The ProcM/ProcA2.8 reaction was incubated for 3 h at 25 °C and the HalM2/HalA2 reaction was incubated at 25 °C for 30 min. For the HalM2/HalA2 reaction, a thrombin-digested His6P-HalA2 substrate was used (Figure S1). Samples were quenched using the standard citrate/TCEP/EDTA quench protocol described in the methods section, C4-SPE

purified, lyophilized and analyzed using the standard LC-ESI-MS conditions. Mass spectra for each peptide sample are shown in Figure S1. These data clearly suggest that our standard citrate quench conditions are sufficient to eliminate the activity of these LanM enzymes during sample workup and prior to LC-ESI-MS analysis of the kinetic samples.

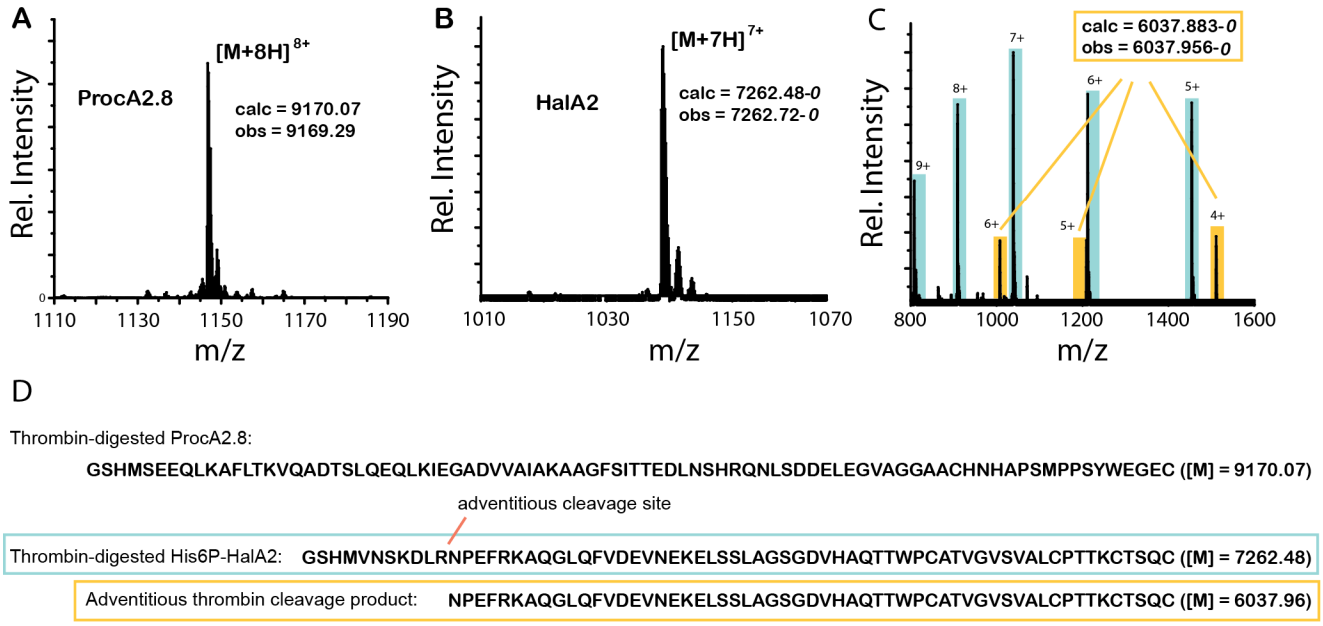

Figure S1. Effect of citrate quench on LanM activity. ESI mass spectra are shown for ProcA2.8 (panel A) and HalA2 (panels B and C) after incubation with ProcM or HalM2, respectively, that had been inactivated in citrate buffer. The inactivated enzymes were unable to modify the wild type substrate peptides under the standard assay conditions described in the Methods, as evidenced by the lack of dehydrated ProcA2.8 and HalA2 peptides. The calculated masses shown in each panel are for the average mass of thrombin-cleaved ProcA2.8 (panel A) and the monoisotopic mass of thrombin-cleaved HalA2 (panel B). Individual isotopes were not resolved for the thrombin-cleaved ProcA2.8 peptide on our Waters Synapt Q/TOF mass spectrometer. Thus, we estimated the average mass ($[M]_{obs}$ = 9169.29), which likely accounts for the discrepancy from the calculated value of $[M]_{avg}$ = 9170.07. The number in italics following the dash in the reported masses in panel B (i.e. "-*0*") denotes the isotope number. By convention, the monoisotopic mass is denoted "0." The complete mass spectrum for the thrombin-digested HalA2 is shown in panel C. Minor signals resulting from the partial adventitious thrombin-mediated cleavage within the HalA2 leader peptide are highlighted in orange. This additional cleavage occurs at the indicated Arg residue shown in panel D. Because of the additional complexity introduced by the adventitious cleavage event, the thrombin cleavage step was omitted for all kinetic experiments. Thrombin (His6P-HalA2) or LysC (ProcA2.8) cleavage was used to identify the peptides associated with the observed ions as described in the next section.

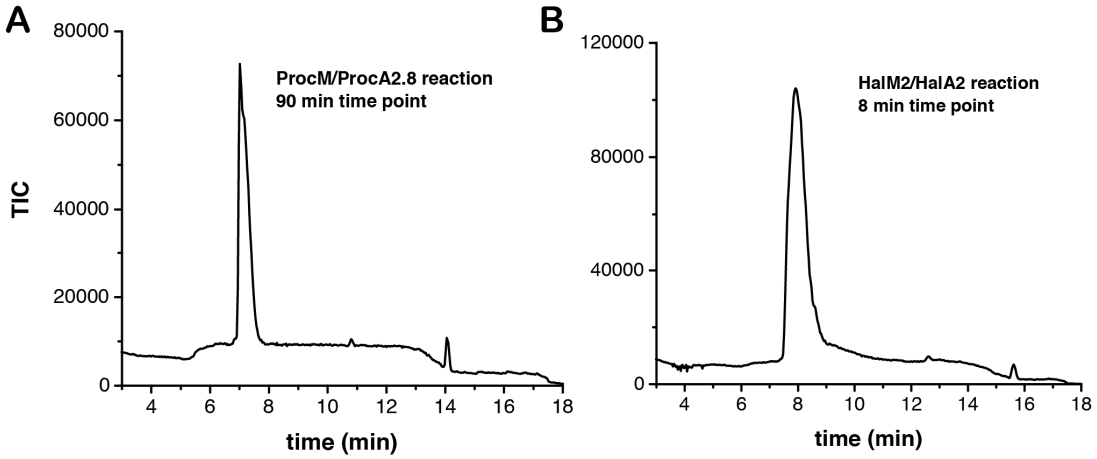

Figure S2. Total ion chromatograms from the 90 and 8 min time points from the ProcM (**A**) and HalM2 (**B**) catalyzed reactions, respectively. All of the peptides present in each reaction mixture eluted as a single, broad peak under our LC conditions. The *y*-axes are in units of total ion counts (TIC).

II. Additional Experiments Related to the Validation of the LC-ESI-MS Kinetic Assay

Assigning intermediates in the HalM2/His$_6$P-HalA2 and ProcM/ProcA2.8 reactions: The relatively large masses (~ 8.5 – 9.5 kDa) of the full-length ProcA2.8 and HalA2 peptides precluded the resolution of their individual isotopic peaks by our Waters Synapt G1 Q/TOF mass spectrometer. To gain more confidence in the assignment of mass spectral signals to specific peptide ions, the 60 and 8 min time points from the kinetic assays of ProcM and HalM2, respectively, were proteolyzed to generate smaller peptides for more accurate mass determination. All of the peptide species that were included in the kinetic models of the HalM2- and ProcM-catalyzed reactions were present at these time points. The ProcM/ProcA2.8 time point was digested with LysC in 100 mM HEPES (pH 7.5), 1 mM EDTA, for 18 h at 4 °C. The HalM2/His$_6$P-HalA2 time point was digested with thrombin in 100 mM HEPES (pH 7.5), 1 mM EDTA, 1 mM TCEP, for 18 h at 4 °C. Following proteolysis, samples were desalted by the standard C4-SPE protocol described in the methods and were lyophilized to dryness. Samples were dissolved in 50 µL of water, diluted to final concentrations of 10 µM (ProcA2.8) or 20 µM (HalA2) total peptide, then analyzed by LC-ESI-MS.

Mass spectra for the proteolyzed HalM2/His$_6$P-HalA2 and ProcM/ProcA2.8 reaction intermediates are shown in Figures S3 and S4, respectively. The data shown in panel A of both figures were collected using the standard LC-ESI-MS conditions employed for the kinetic assays (see methods section). To obtain more accurate mass assignments for the relevant peptide species, MS data were additionally collected for the ProcM/ProcA2.8 reaction sample with the following instrument settings on the Synapt G1 Q/TOF instrument: positive ion mode, V optics, capillary voltage = 3.0 kV, cone gas = 206 L/h, desolvation gas = 600 L/h, source temperature = 120 °C, desolvation temperature = 300 °C. Data were collected over an m/z window of 50 – 2000 in continuous mode with a 1 s scan rate (0.02 s interscan time), and a Glu-fibrinopeptide B (Sigma) lockspray solution for internal calibration. Spectra were smoothed and deconvoluted using the MaxEnt3 function of the MassLynx software package to determine the observed monoisotopic ion masses shown in

Figure S4B and Table S2. For the HalM2/His_6P-HalA2 reaction, MS data were additionally collected on a Synapt G2-Si instrument at the Mass Spectrometry core facility at the University of Illinois, Urbana-Champaign, with the following instrument settings: positive ion mode, W optics, capillary voltage = 0.5 kV, cone gas = 60 L/h, desolvation gas = 600 L/h, temperature = 120 °C, desolvation temperature = 300 °C. Data were collected over an m/z window of 500 – 2000 in continuous mode with a 0.2 s scan rate (0.015 s interscan time) using a leucine-enkaphalin lockspray solution for internal calibration. Spectra were smoothed and deconvoluted using the MaxEnt3 function of the MassLynx software package to determine the observed monoisotopic ion masses shown in Figure S3B and Table S1. The theoretical monoisotopic masses shown in Tables S1 and S2 were calculated from the putative molecular formula of the peptide using the MS isotope server available from the University of California, San Francisco website (http://prospector.ucsf.edu/prospector/cgi-bin/mssearch.cgi).

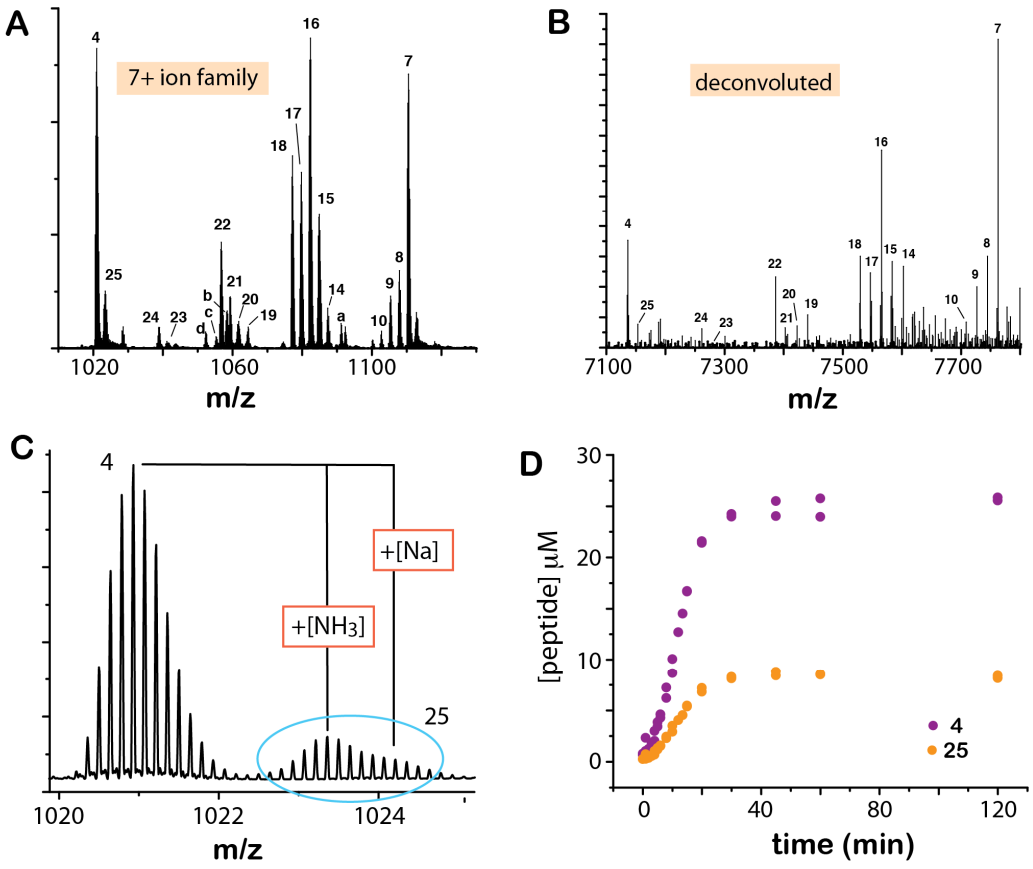

Figure S3. A) Electrospray ionization mass spectrum for the thrombin-digested 8 min time point from the HalM2/His_6P-HalA2 reaction after treatment with *N*-ethylmaleimide (NEM). The spectrum for the 7^+ ion family is shown. Species **a**, **b**, **c**, and **d** are the 6+ ions of species **7**, **16**, **17**, **18**, respectively, that have been adventitiously cleaved by thrombin at the site in the HalA2 leader peptide indicated in Figure S1D. The deconvoluted mass spectrum of this sample (reanalyzed on a Synapt G2-Si instrument) is shown in panel B. The observed monosiotopic masses and peak assignments are given in Table S1. C) Signal **25** (shown here as its 7+ ion) is likely a mixture of two species – the sodium and ammonia adducts of compound **4**. Signal **25** was treated as a single species and was combined with the signal for the final product (compound **4**) during kinetic analysis. The plot in panel D shows that compounds **4** and **25** exhibit very similar kinetics, which is expected if signal **25** is composed of adducts of **4**. Hence, regardless of the exact identity of **25**, its treatment in the model is supported by the kinetic data.

Table S1. Peak assignments for the peptide ions observed in the thrombin-digested 8 min time point from the HalM2/His_6P-HalA2 reaction. The structures of selected compounds are also shown below the Table.

compound*	assignment″	Monoisotopic Masses theoretical	observed	error (ppm)
4	[M+4Lan+3Dhx]	7136.412	7136.443	4
25°	[M+4Lan+3Dhx+NH_3]	7153.439	7153.461	3
	[M+4Lan+3Dhx+Na]	7159.402	7159.430	4
24	[M+3Lan+4Dhx+NEM]	7261.460	7261.505	6
23	[M+3Lan+3Dhx+NEM]	7279.470	7279.473	0.4
22	[M+2Lan+5Dhx+2NEM]	7386.507	7386.550	6
21	[M+2Lan+4Dhx+2NEM]	7404.518	7404.566	6
20	[M+2Lan+3Dhx+2NEM]	7422.529	7422.547	2
19	[M+2Lan+2Dhx+2NEM]	7440.539	7440.534	0.7
18	[M+Lan+5Dhx+3NEM]	7529.565	7529.622	8
17	[M+Lan+4Dhx+3NEM]	7547.576	7547.639	8
16	[M+Lan+3Dhx+3NEM]	7565.587	7565.637	7
15	[M+Lan+2Dhx+3NEM]	7583.599	7583.599	0
14	[M+Lan+1Dhx+3NEM]	7601.608	7601.576	4
13′	[M+Lan+3NEM]	7619.619	7619.558	8
12′	[M+3NEM]	7636.603	7636.590	2
11′	[M+4Dhx+4NEM]	7690.635		
10	[M+3Dhx+4NEM]	7708.645	7708.690	6
9	[M+2Dhx+4NEM]	7726.656	7726.691	4
8	[M+1Dhx+4NEM]	7744.666	7744.710	6
7	[M+4NEM]	7762.677	7762.731	7

*For ease of presentation, the compound numbering for the thrombin-digested His_6P-HalA2 species presented in this table is the same as the numbering used throughout the main text when describing the full-length, non-proteolyzed His_6P-HalA2 species.

″M = thrombin-cleaved His_6P-HalA2 (m/z = 7262.486-*0*); Lan = lanthionine or methyllanthionine (-18.011 Da); Dhx = dehydroalanine or dehydrobutyrine (-18.011 Da); NEM = *N*-ethylmaleimide (+125.048 Da); O = oxidation (+15.995 Da)

′ Minor species that were not included in the kinetic models reported in this study.

° Signal **25** is likely a mixture of the ammonia and Na adducts of the final product, compound **4**. See the legend of Figure S3 for additional details.

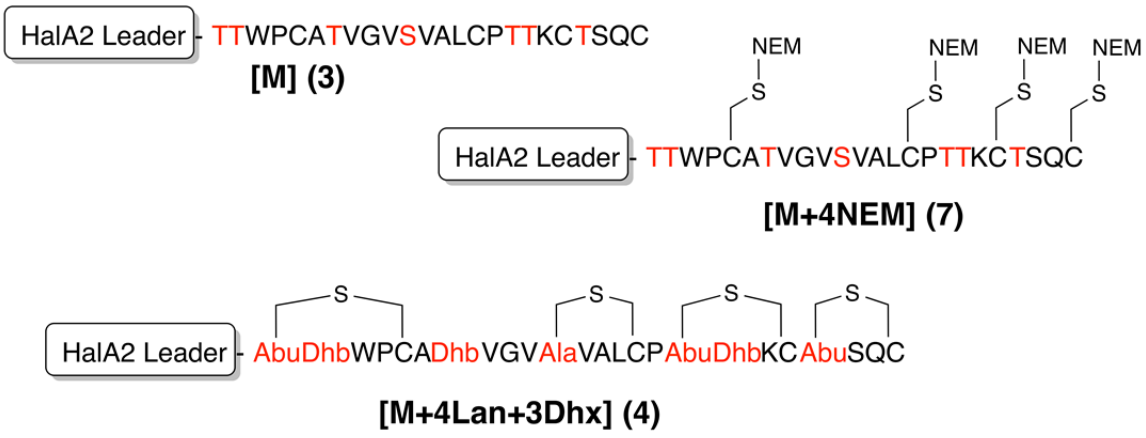

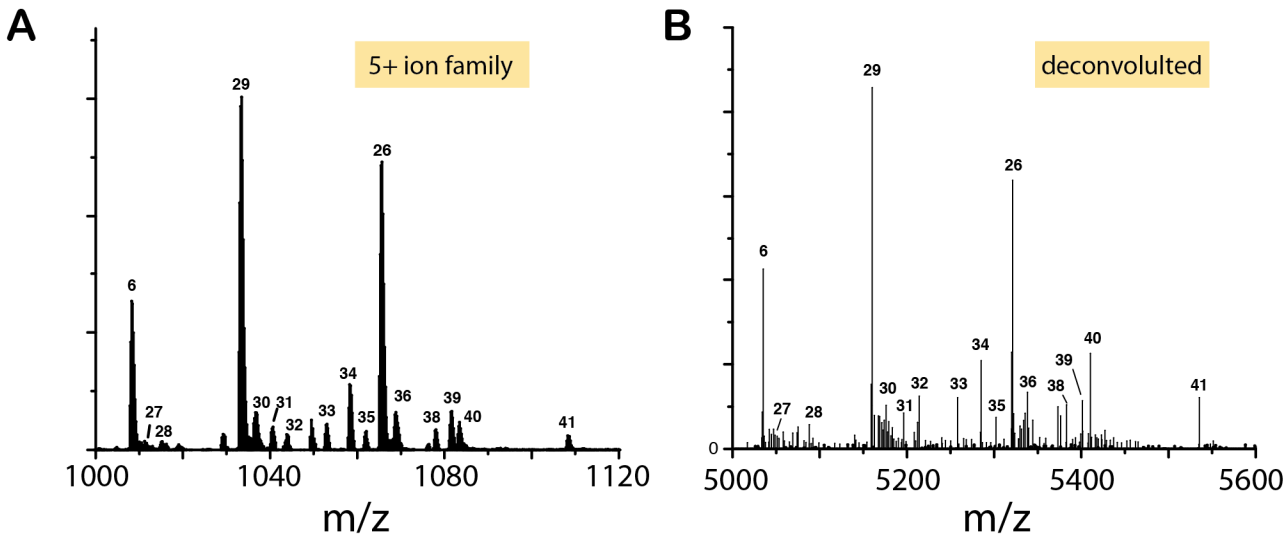

Figure S4. Electrospray ionization mass spectra for the LysC-digested 60 min time point from the ProcM/ProcA2.8 reaction after treatment with NEM. The data in panel A show the 5+ ion family and were collected under the same LC-ESI-MS conditions that were used for the kinetic assays. For more accurate mass determination, the sample in (A) was reanalyzed under slightly different LC-ESI-MS conditions (see the "Assigning intermediates in the HalM2/His_6P-HalA2 and ProcM/ProcA2.8 reactions" section of the SI). The data were deconvoluted to give the monoisotopic masses shown in panel B and Table S2. All ions could be assigned (Table S2) except for two very low intensity species, **28** and **32** (m/z = 5088.063 and 5214.101, respectively). These ions were not included in the simulated kinetic model for the ProcM/ProcA2.8 reaction.

Table S2. Peak assignments for the LysC-digested 60 min time point from the ProcM/ProcA2.8 reaction. The structures of selected compounds are also shown below the Table.

compound*	assignment″	Monosiotopic Masses theoretical	observed	error (ppm)
6	[M+2Lan]	5035.174	5035.177	0.6
27	[M+2Lan+O]	5051.169	5051.145	5
28			5088.063°	
29	[M+Lan+Dha+NEM]	5160.222	5160.212	2
30	[M+Lan+Dha+O+NEM]	5176.217	5176.283	1
31	[M+NEM]	5196.243	5196.218	5
32			5214.101°	
33	[M+Lan+P+NEM]	5258.199	5258.178	4
34	[M+2Dha+2NEM]	5285.269	5285.223	9
35	[M+Dha+2NEM]	5303.280	5303.240	8
26	[M+2NEM]	5321.291	5321.327	7
36	[M+O+2NEM]	5337.285	5337.199	16
38	[M+P+Dha+2NEM]	5383.246	5383.223	4
39	[M+P+2NEM]	5401.257	5401.184	14
40	[M+Lan+Dha+TCEP+NEM]	5410.282	5410.258	4
41	[M+2Dha+TCEP+2NEM]	5535.330	5535.297	6

*For ease of presentation, the compound numbering for the LysC-digested ProcA2.8 species presented in this table is the same as the numbering used throughout the main text when describing the full-length, non-proteolyzed ProcA2.8 species.
″M = LysC digested ProcA2.8 (m/z = 5071.195-*0*); Lan = lanthionine (-18.011 Da); Dha = dehydroalanine (-18.011 Da); NEM = *N*-ethylmaleimide (+125.048 Da); O = oxidation (+15.995 Da); TCEP = tris(2-carboxyethyl)phosphine (+ 250.061 Da); P = phosphate (+79.966 Da).
°See Figure S4 legend.

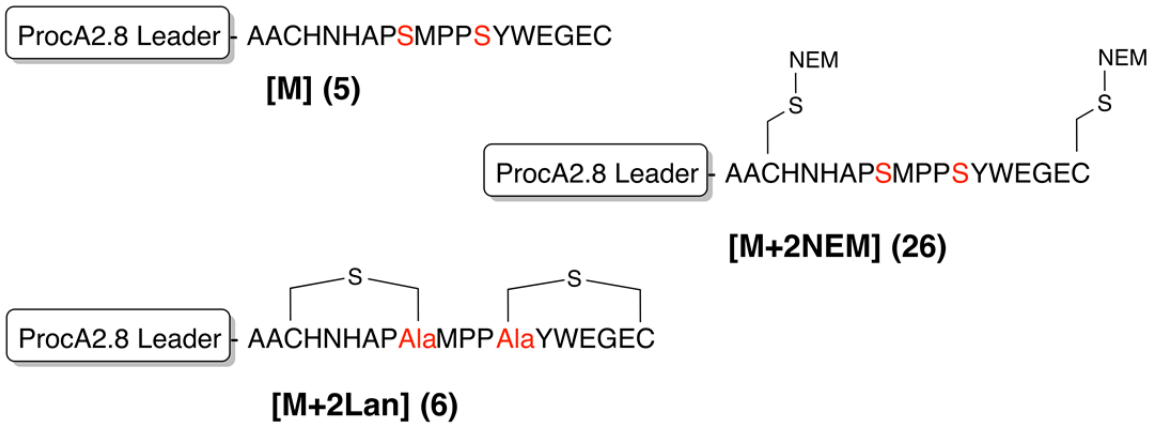

Linear ranges for LC-ESI-MS assays: For studies with the unmodified peptides, the concentrations of the thrombin digested ProcA2.8 and non-digested His_6P-HalA2 peptides were determined using their calculated extinction coefficients at 280 nm (7115 M^{-1} cm^{-1} and 5500 M^{-1} cm^{-1}, respectively). Serial dilutions of peptide samples were made in duplicate in LC solvent (50% MeCN in H_2O, 0.1% formic acid) and were analyzed by LC-ESI-MS in randomized order. Similarly, for determination of the linear signal ranges of reaction intermediates, portions of the 8 and 90 min time points from the HalM2 and ProcM kinetic reactions, respectively, were first diluted to 20 μM or 10 μM total peptide, respectively, and were then serially diluted.

Data were collected and analyzed using the standard LC-ESI-MS conditions given in the Methods section. For each sample, extracted ion chromatograms (EICs) for each detectable multiply charged ion of each relevant peptide were generated, integrated, and summed together to give the total signal for that particular peptide ($\sum A_{x,i}$), which was then plotted versus peptide concentration and fitted with a line. Linear fits are shown in Figure 2 of the main text and in Figures S5 (for His_6P-HalA2-derived peptides) and S6 (for ProcA2.8-derived peptides).

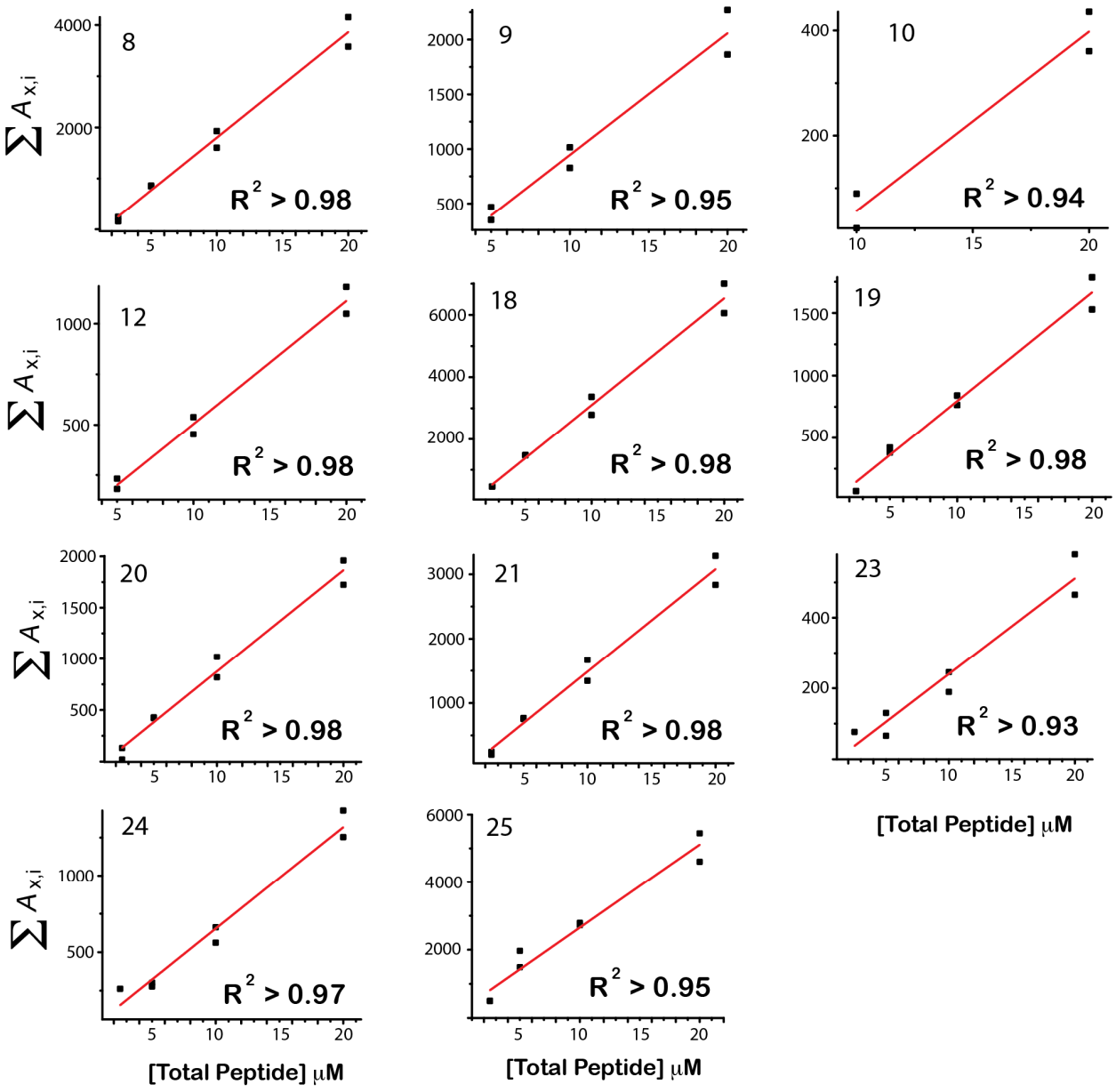

Figure S5. Linear fits of LC-ESI-MS signal vs. peptide concentration for His_6P-HalA2-derived peptides. Compound numbers correspond to the ions shown in Figure 1B, and the identity of each compound is listed in Table S1. The linear ranges for additional reaction intermediates are shown in Figure 2 of the main text.

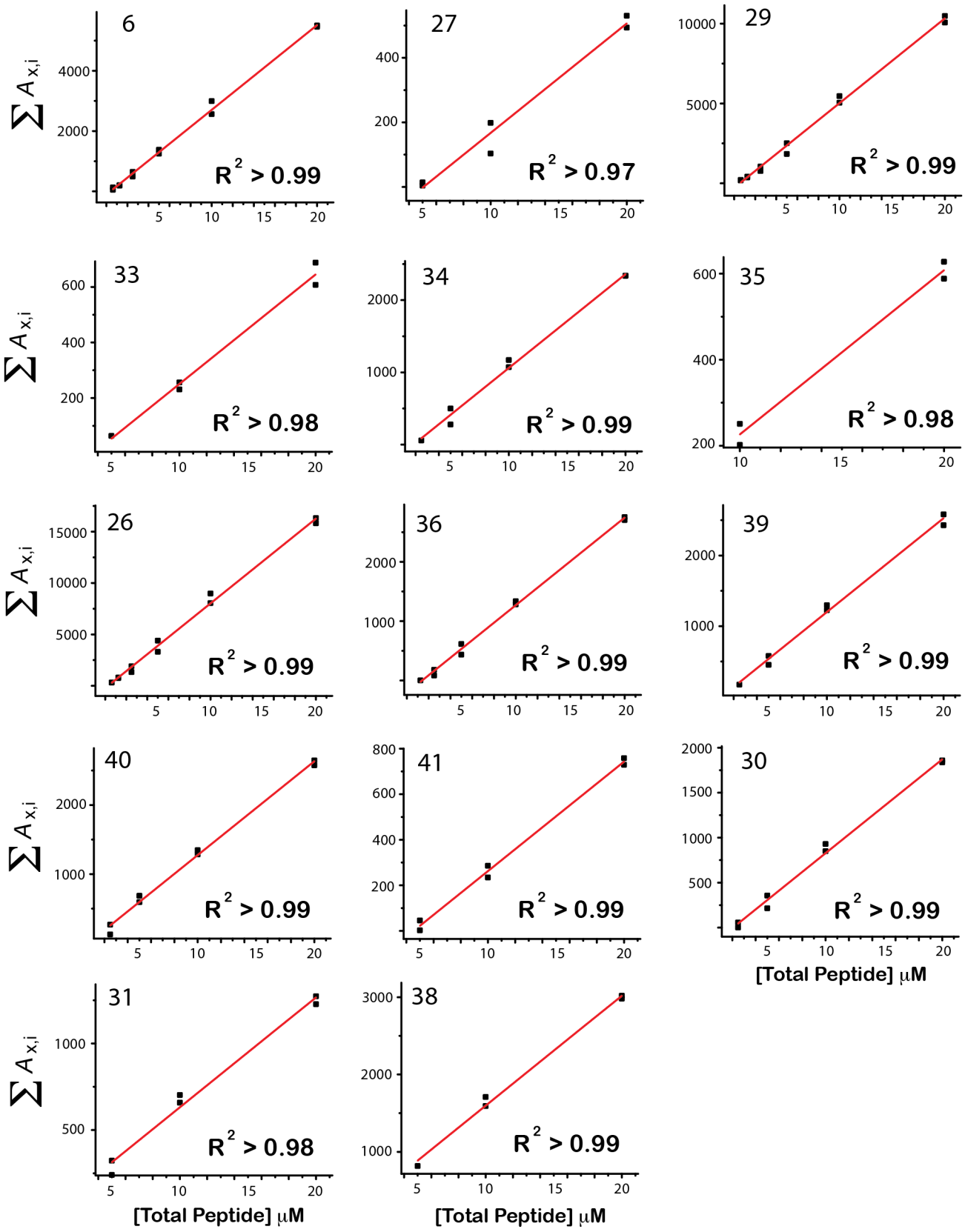

Figure S6. Linear fits of LC-ESI-MS signal vs. peptide concentration for ProcA2.8-derived peptides. Compound numbers correspond to the ions shown in Figure 1D, and the identity of each compound is listed in Table S2.

Table S3. Effect of NEM alkylation on peptide ionization efficiency

HalM2/His$_6$P-HalA2 Reaction

	Fractional Abundance (F_x)*					
	Replicate 1		Replicate 2		Average ± S.E.°	
species′	**- NEM**	**+ NEM**	**- NEM**	**+ NEM**	**- NEM**	**+ NEM**
A or (4+24+22)	0.217	0.209	0.219	0.189	0.218 ± 0.001	0.20 ± 0.01
B or (25+23+21+18)	0.154	0.159	0.145	0.151	0.149 ± 0.004	0.155 ± 0.004
C or (20+17)	0.111	0.097	0.103	0.095	0.107 ± 0.004	0.096 ± 0.001
D or (19+16+11)	0.163	0.159	0.160	0.162	0.161 ± 0.002	0.160 ± 0.001
E or (15+10)	0.079	0.092	0.076	0.094	0.076 ± 0.001	0.093 ± 0.001
F or (14+9)	0.043	0.056	0.043	0.060	0.0428 ± 0.0002	0.058 ± 0.002
G or (13+8)	0.037	0.052	0.042	0.055	0.039 ± 0.002	0.053 ± 0.002
H or (12+7)	0.197	0.177	0.213	0.194	0.21 ± 0.01	0.19 ± 0.01

ProcM/ProcA2.8 Reaction

	Fractional Abundance (F_x)					
	Replicate 1		**Replicate 2**		**Average ± S.E.**	
species	**- NEM**	**+ NEM**	**- NEM**	**+ NEM**	**- NEM**	**+ NEM**
I or (6+29+34)	0.393	0.435	0.397	0.427	0.395 ± 0.002	0.431 ± 0.004
J or (27+30+35)″	0.097	0.122	0.103	0.119	0.100 ± 0.003	0.121 ± 0.001
K or (31+26)	0.208	0.256	0.226	0.253	0.22 ± 0.01	0.254 ± 0.001
L or (28+32+36)	0.102	0.082	0.107	0.082	0.105 ± 0.002	0.082 ± 0.0002
M or (33+38)	0.044	0.029	0.041	0.026	0.042 ± 0.002	0.027 ± 0.002
N or 39	0.044	0.035	0.043	0.032	0.044 ± 0.001	0.033 ± 0.001
O or (40+41)	0.112	0.063	0.084	0.060	0.10 ± 0.01	0.062 ± 0.001

*The fractional abundance values were calculated as described in the Methods section of the main text.
°S.E. – standard error of the mean
′The capital letters correspond to groups of isobaric species as indicated in Fig. 3 of the main text.
″The J group of peptides contains species that are dehydrated once (**35**) as well as species that are dehydrated twice and oxidized (**27** and **30**). These modifications lead to mass differences from the starting material of -18 (for species **35**) and of -20 Da (for species **27** and **30**) that could not be resolved in the spectra shown in Figure 3C. However, upon NEM alkylation (Figure 3D) and LysC digestion (Figure S4, Table S2), species **27**, **30**, and **35** are resolved and their assignments become clear.

Preparation of a phosphorylated ProcA2.8 derivative: We constructed a ProcA2.8 variant (dubbed ProcA2.8-S13) that lacks both the Cys residues (C3 and C19) as well as the *N*-terminal most Ser residue (S9) present in the wt ProcA2.8 core peptide. Using the *procA2.8/pET15* construct described above as the template, the codons for these three residues were each mutated to Ala codons by GenScript USA, Inc. (Piscataway, NJ.). The resulting plasmid was used to transform *E. coli* BL21 (DE3) and the peptide was expressed, IMAC purified, thrombin-digested, and purified by HPLC in a manner identical to that described in the "*Preparation of LanA peptides"* sections above. The purified ProcA2.8-S13 peptide was then incubated with a ProcM variant (ProcM-T516A) that catalyzes phosphorylation, but that is much attenuated in its ability to eliminate the phosphate to generate Dha residues.[7] The 5 mL reaction was conducted under the standard ProcM assay conditions given in the main text, except that the enzyme concentration was increased to 10 μM. After an 18 h incubation at 25 °C, TFA was added to 0.1% (v/v) to quench the reaction and the sample was once again

purified by C4-SPE and RP-HPLC. Using these conditions, we were able to generate a pure sample of ProcA2.8-pS13 for further studies (Figure S7, panels A and B).

Determining the effect of phosphorylation on ProcA2.8 ionization efficiency: The concentrations of the ProcA2.8-S13 and ProcA2.8-pS13 peptide stock solutions were determined by UV-visible absorption to be 202 $\pm$ 0.5 μM and 361 $\pm$ 1 μM, respectively, assuming an extinction coefficient of 7,115 M^{-1} cm^{-1} for both peptides. A mixture containing 8 μM ProcA2.8-S13 and 4 μM ProcA2.8-pS13 was prepared in LC-ESI-MS injection solvent (50% MeCN in 0.1% formic acid) and was then serially diluted into an identical sample lacking ProcA2.8-S13. In this way, we generated a set of standard samples containing 4 μM ProcA2.8-pS13 and variable concentrations of ProcA2.8-S13 (from 0.5 to 8 μM). These samples were subjected to LC-ESI-MS using conditions identical to those used for the kinetic assays. The mass spectrum of the peptide mixture containing 4 μM of each peptide is shown in Figures S7C and S7D. For each standard sample, we determined the total EIC peak area for both peptides ($\sum A_{x,i}$) as described in the methods section and then plotted the ratio of these values vs. the known concentration ratio to give the plot shown in Figure S7E. A linear fit of this data yielded a slope of 1.02 $\pm$ 0.03 (R^2 > 0.99), suggesting that the ionization efficiencies of the two peptides are within error of each other. Thus, phosphorylation does not seem to detectably alter the LC-ESI-MS signal of full-length ProcA2.8-derived peptides under the conditions of and at the concentrations used in our kinetic assay.

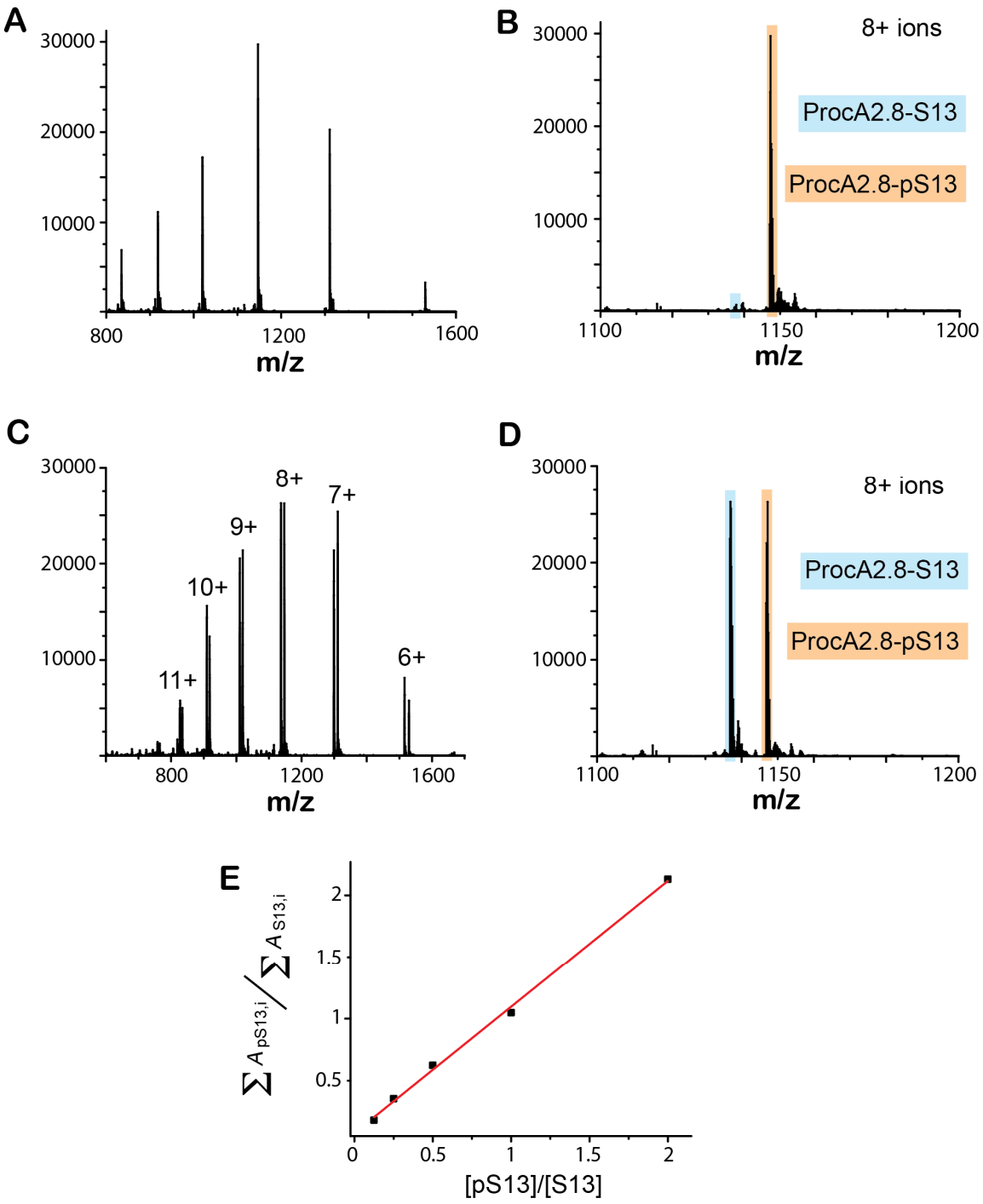

Figure S7. ESI-MS spectrum of the enzymatically-prepared and HPLC-purified ProcA2.8-pS13 ($[M]_{calc}$ = 9169.364-*5*, $[M]_{obs}$ = 9169.460-*5*) is shown in panels A and B. A very small amount of non-phosphorylated starting peptide is also observed (highlighted in blue). The ESI-MS spectrum of a mixture containing 4 μM each of ProcA2.8-S13 and ProcA2.8-pS13 is shown in panels C and D. The ratio of the EIC peak areas of both peptides for mixtures of the two peptides present in different concentrations (see SI text), summed over the +6 to +10 charge states, is plotted vs. the known concentration ratio and fitted with a line in panel E (slope = 1.02 ± 0.02, R^2 > 0.99).

III. Additional Experiments Related to the Kinetic Characterization of HalM2

Construction of a fluorescently labeled HalA2 peptide for determination of the HalM2/HalA2 binding affinity: We used a native chemical ligation (NCL) approach to generate a fluorescently labeled HalA2 construct for determination of the HalM2/HalA2 binding affinity. The structure of this construct is shown in Figure S8A. The approach involved the coupling of a synthetic peptide harboring an *N*-terminal fluorescein tag and a *C*-terminal thioester with a biosynthetically-generated HalA2 variant containing a Cys residue on the *N*-terminus (dubbed HalA2-Cys). The synthetic peptide was chemically synthesized using Fmoc-based solid phase peptide synthesis (SPPS) under a constant nitrogen stream. Rink amide resin (50 μ mol) was first washed with dimethylformamide (DMF) (3 x 5 mL), methylene chloride (CH_2Cl_2) (3 x 5 mL), and DMF (3 x 5 mL). The amide resin was then treated with 20% piperidine/DMF (3 x 5 mL x 5 min), and washed. A solution of Fmoc-Glu-*O*-Allyl amino acid (4 equiv), PyAoP (4 equiv) and NMM (8 equiv) in DMF was pre-activated for 4 min, then added to the resin and incubated for 2 h. This process links the Glu to the resin via its side chain carboxylate and leaves the Glu α-carboxylate protected with an allyl group. Amino acids were then iteratively added to the *N*-terminus of the peptide on the resin using the same procedure. After deprotection of the last amino acid, NHS-Fluorescein and DIPEA (each 2 equiv in DMF) were added to the resin and reacted for 3 h. The resin was then washed as described above. The *C*-terminal allyl-ester was deprotected with tetrakis(triphenylphosphine) palladium (1 equiv) and phenylsilane (2.5 equiv) in CH_2Cl_2 for 1 h. This deprotection was repeated once. The resin was then washed again before treatment with ethyl-3-mercaptopropionate, HOBt, and N,N'-diisopropylcarbodiimide in CH_2Cl_2:DMF (4:1) for 1 h. Following another wash step, the final global deprotection and cleavage of the synthetic peptide from the resin was achieved with TFA/TIPS/water (18:1:1 (v/v/v), 5 mL) for 2 h. The peptide was filtered and the TFA was removed with a nitrogen stream. The remaining peptide was precipitated with ether and collected by centrifugation. The crude peptide was purified by HPLC using a Phenomenex Luna C-18 semi-preparative column (10 µm particle size, 250 mm × 4.6 mm, 100 Å) at a flow rate of 8 mL min^{-1}. The mobile phase, consisting of 0.1% trifluoroacetic acid (solvent A) in water and 0.1% TFA in acetonitrile (solvent B), was altered from 0% to 100% solvent B over 50 min. The identity of purified fluorescein-Strep tag-thioester was assessed with MALDI-ToF MS ($[M]_{calc}$ = 1803.9, $[M]_{obs}$ = 1803.2, data not shown) and the peptide was stored at -80 °C. To make the HalA2-Cys construct, the *halA2/pET15* plasmid was mutated to contain a cysteine at position 2 of the His-tag (see Figure S8A) using standard site directed mutagenesis protocols to make the construct HalA2-Cys/pET15. The HalA2-Cys peptide was over-expressed in *E. coli* and purified as described for the other LanA peptides. During expression in *E. coli*, the *N*-terminal Met was cleaved from the recombinant HalA2-Cys peptide, leaving a product with an *N*-terminal Cys residue suitable for native chemical ligation.

Native chemical ligation and purification: The native chemical ligation was performed as described previously.[8] Briefly, synthetic fluorescein-strep-tag *C*-terminal thioester (3 mM) and expressed and purified HalA2-Cys (3 mM) were re-suspended in degassed and filtered buffer containing 6 M guanidine hydrochloride, 0.1 M

Na_2HPO_4, 50 mM 4-mercaptophenylacetic acid (MPAA), and 20 mM TCEP (pH 7.0). The vessel was purged with nitrogen for 15 min, then incubated overnight at room temperature. The NCL reaction was then purified by IMAC (to remove the unreacted, fluorescein-labeled peptide) and the eluent was directly applied to Strep-Tactin Plus beads (Qiagen) and gently rocked for 2 h to allow binding. The beads were washed with 10 column volumes

(CV) of buffer NP (50 mM NaH_2PO_4, 300 mM NaCl, pH 8.0) to remove unreacted HalA2-Cys peptide. The NCL product was then eluted with 3 CV of NPD buffer (50 mM NaH_2PO_4, 300 mM NaCl, 2.5 mM desthiobiotin, pH 8.0), desalted using a C4-SPE column and lyophilized. The mass of the final, fluorescein-labeled HalA2 construct ($HalA2_{fluor}$) was verified by MALDI-ToF MS (Figure S8B, $[M]_{calc}$ = 10733, $[M]_{obs}$ = 10736).

Fluorescence polarization (FP) assay to determine HalM2:HalA2 binding affinity: FP was performed on a Synergy H4 Hybrid plate reader (BioTek; Winoski, VT) and the data were recorded with Gen5 software. Increasing concentrations of HalM2 were added to $HalA2_{fluor}$ (20 nM) in FP buffer (50 mM HEPES, 10 mM $MgCl_2$, 1 mM TCEP, 0.25 mM AMP-PNP, pH 7.5). Each binding assay was repeated in triplicate in a 96 well plate (CoStar 3615). FP signals were corrected for scattering, plotted vs. [HalM2], and were fitted with a hyperbola as discussed below in the "*Fluorescence polarization assay to measure the ProcM:ProcA2.8 binding affinity*" section in order to determine a K_d of 1.8 ± 0.2 μM (Figure S8C).

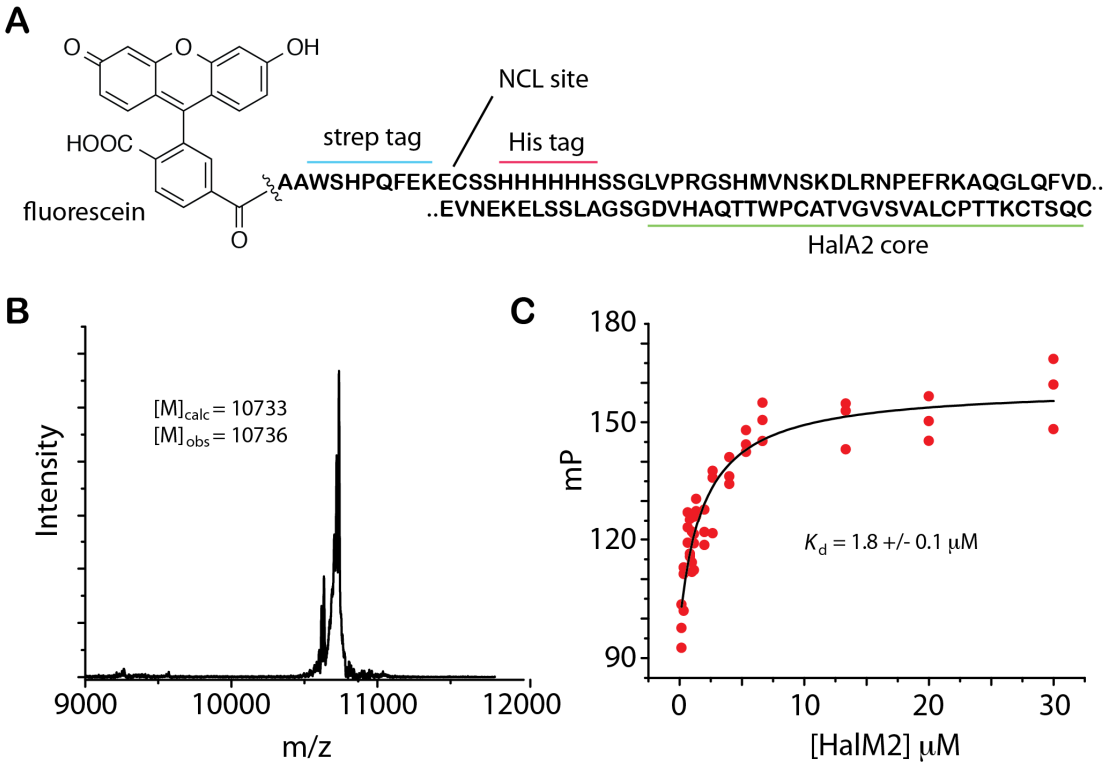

Figure S8. Determining the HalM2/$HalA2_{fluor}$ binding constant. A) The structure of $HalA2_{fluor}$ - the fluorescein-labeled HalA2 construct used in this study. B) MALDI-ToF MS spectrum of the HPLC-purified $HalA2_{fluor}$ construct used in the titration studies. C) The binding affinity of HalM2/$HalA2_{fluor}$ was determined by fluorescence polarization.

Single molecule fluorescence measurements of HalM2:His_6P-HalA2 dissociation rate: In order to estimate the dissociation rate for the HalM2:His_6P-HalA2 bimolecular complex, we devised a single molecule fluorescence binding experiment. In this experiment, total internal reflection fluorescence (TIRF) microscopy was used to measure the lifetime of the HalM2:His_6P-HalA2 interaction by direct observation of the binding of fluorescently-labeled HalM2 molecules to a lawn of unlabeled His_6P-HalA2 peptide coated on a polyethylene glycol (PEG) passivated quartz surface.

Non-specific labeling of HalM2: His_6-HalM2 was labeled non-specifically on Cys thiol residues with AlexaFluor 647 (AF647)-maleimide (Invitrogen) by spiking a 100 μL sample of HalM2 (64 μM) in storage buffer (25 mM Tris, 500 mM NaCl, 10 % glycerol, pH 8.0) with 5 μL of a 10 mg/mL AF647 solution (in DMF) to give a final dye concentration of 366 μM. The labeling reaction was incubated at 4 °C for 4 h. At this point, the mixture was transferred to a 0.5 mL Slide-A-Lyzer dialysis cassette (Thermo Scientific, 5 kDa cutoff) and 5 units of thrombin (MP Biomedicals) were added to remove the *N*-terminal His_6 tag from the His_6-LanM constructs. Following over night dialysis at 4 °C against 4 L of storage buffer, residual free dye and the proteolyzed *N*-terminal His_6-tag were removed using an Amicon Ultra Centrifugal Filter device with a 100 kDa MW cutoff (Milipore). Following centrifugation, the retentate was diluted with storage buffer and re-centrifuged. This process was repeated several times. The concentration of protein and label were measured by UV-visible absorption spectroscopy using extinction coefficients of 120,000 $M^{-1}cm^{-1}$ at 280 nm and of 239,000 $M^{-1}cm^{-1}$ at 650 nm for HalM2 and AF647, respectively. The labeled enzyme (herein termed 647-HalM2) was diluted to 1 μM, flash frozen in small aliquots in liquid nitrogen, and stored at -80 °C until use. The 647-HalM2 enzyme exhibited similar activity to the unlabeled enzyme (data not shown).

Preparation of His_6P-HalA2-coated PEG slides: Quartz slides and glass coverslips were passivated with biotinylated-PEG (LaysanBio) as described previously[9] and stored under vacuum at -80 °C until use. Immediately prior to conducting single molecule experiments, the coverslip was fixed onto the quartz slide using double-sided tape in order to make several observation channels on the slide. After fixing the coverslip, the channels were incubated for 5 min with 0.05 mg/mL NeutrAvidin (NA, Thermo Scientific) in single molecule (sm) buffer (100 mM HEPES, 100 mM NaCl, 1 mM Trolox (6-hydroxy-2,5,7,8-tetramethylchroman-2-carboxylic acid), 0.1 mg/mL BSA, pH 7.5). The channels were then washed and incubated with sm-buffer for 30 min. At this point, sm-buffer containing a 1:100 dilution of biotinylated anti-His_6 antibody (penta-his biotin conjugate, Qiagen) was introduced into the appropriate channels and incubated for 5 min. Channels were then washed with approximately 10 volumes (150 μL) of sm-buffer prior to adding a solution containing 1 μM His_6P-HalA2 (when present) and 0.5 mM TCEP in sm-buffer. The peptide solution was incubated on the surface for at least 15 min prior to imaging to allow the His_6-tagged peptide sufficient time to bind to the immobilized anti His_6-antibody. For the experiments described below, negative control channels lacking either antibody or His_6P-HalA2 peptide were prepared and analyzed in parallel in order to determine the degree of non-specific 647-HalM2 surface binding.

Single molecule binding experiments and imaging conditions: In order to establish a relationship between the number of surface-bound 647-HalM2 molecules and the [647-HalM2] concentration, a series of solutions containing variable amounts of 647-HalM2 (62.5, 125, 250, 500, 1000 pM) were prepared by serial dilution of a 1 nM 647-HalM2 stock solution in sm-buffer supplemented with 0.5 mM TCEP and 5 mM $MgCl_2$. Immediately prior to imaging, the channel to be imaged was washed with 150 μL of sm-buffer to remove excess LanA peptide that was not bound to the surface. A 100 μL aliquot of the appropriate enzyme solution was then spiked with 2 μL of 50 % (w/v) glucose and 1 μL of a "gloxy" stock solution containing glucose oxidase (Sigma) and bovine liver catalase (Calbio) to remove O_2 from the imaging buffer. When appropriate, an additional 1 μL portion of 500 mM adenosine 5′-triphosphate (ATP, Sigma) or adenosine 5′-(β,γ-imido)triphosphate (AMP-PNP, Sigma) was also added at this point. The final composition of the imaging mixture was variable [647-HalM2] in 100 mM HEPES, 100 mM NaCl, 5 mM $MgCl_2$, 5 mM ATP (or AMP-PNP, when present), 0.5 mM TCEP, 0.1 mg/mL BSA, 1 mM Trolox, 1% glucose, 1 mg/mL glucose oxidase, and 100 units of catalase, pH 7.5. This solution was then quickly transferred to the appropriate channel of the PEG slide for the imaging of single molecule binding events. Slides were mounted on a custom-built prism type TIRF instrument.[9] Surface-immobilized 647-HalM2 molecules were excited with 632 nm laser light, and fluorescent photons were directed to an Andor iXon EMCCD camera (Andor Technology, Belfast, Ireland) for detection of spatially resolved single molecules on the PEG surface. For data acquisition, constant gain and background fluorescence correction were used for all experiments, and all images were collected with a frame rate of 10 frames/s. All data were processed and analyzed using custom software written in IDL and Matlab.[9]

Binding properties of HalM2: For each condition, we recorded several 2 s movies in order to count the number of 647-HalM2 molecules bound to the surface. To each channel, the 647-HalM2 solutions were added in order from the most dilute sample (62.5 pM) to the most concentrated (1 nM). As can be seen in Figure S9, efficient surface binding of 647-HalM2 requires both the anti His_6-antibody and the His_6-HalA2 peptide, suggesting that the majority of the fluorescing spots observed on our surface are due to specific binding interactions between HalM2 and His_6P-HalA2, rather than to non-specific binding of 647-HalM2 to the surface. In addition, the similar molecule counts under conditions with and without ATP (or AMP-PNP) suggest that nucleotide binding has only a minimal effect on the HalM2 surface binding rate. This observation suggests that ATP binding likely does not drastically alter k_{on} for the bimolecular association of HalM2 and His_6P-HalA2 in solution.

After recording the 2 s movies for the 125 pM 647-HalM2 condition, we also recorded two longer movies (120 s) in each channel in order to measure the average surface residence time (τ_{on}) of transiently-bound 647-HalM2 molecules (Figure S10), and whether or not τ_{on} was affected by the presence of ATP or AMP-PNP. The representative Movie 1 (see separate Supporting Information Data file) shows transient 647-HalM2 binding events to a surface coated with His_6P-HalA2. Numerous single molecule binding events, such as those depicted in Figure S10A and B, were observed under these conditions (typically several thousand binding events per 120 s movie). Single molecule binding events were scored by the following criteria (see Figure

S10): 1) the binding event had to be transient and last for more than 1 frame (> 100 ms), 2) the AF647 fluorescence had to exceed a threshold of 500 photon counts/frame, 3) the molecule had to exhibit single step binding and dissociation, and 4) the molecule could not exhibit multi-step photobleaching. Using these criteria, the τ_{on}values for approximately 1000 647-HalM2 binding events were measured for the conditions containing ATP, AMP-PNP, or no nucleotide. The τ_{on}values were then fitted with exponential decay functions to estimate the magnitude of the rate constant for HalM2:His_6P-HalA2 dissociation (Figure S11 and Table S4). For all conditions, the data were best fit with a double exponential function, suggesting the presence of two kinetically significant dissociation rates. The double exponential fits consistently gave smaller R^2 values and residuals that were more evenly spaced around the origin than single exponential fits (Figure S11B).

Overall, the fitted parameter estimates were very similar - regardless of the presence of ATP or AMP-PNP in the reaction mixture (Table S4). Once again, this suggests a minimal effect of ATP binding on the affinity of HalM2 for His_6P-HalA2. There appears to be a slight increase in the magnitude of the fast phase rate constant, k_f, in the presence of ATP or AMP-PNP. We attempted to simulate our kinetic data with a dissociation rate approximated by k_f = 170 min^{-1}, but we were consistently unable to accurately reproduce the early phases of the kinetic time course under these simulation conditions. Tentatively, we assign this faster rate to the dissociation of non-productively bound 647-HalM2 or to the dissociation rate for a non-specific interaction of 647-HalM2 with the surface. It is not clear why k_f would increase in the presence of nucleotide. In contrast, there appears to be a slight, but significant, decrease in the slow phase rate constant k_s in the presence of ATP, indicating a slightly more stable HalM2:His_6P-HalA2 interaction under these conditions. As everything is present in this reaction for HalM2 to modify surface-bound His_6P-HalA2, the slower k_s could indicate the presence of catalytically competent HalM2:His_6P-HalA2 complexes that are actively undergoing peptide modification. Active modification would be expected to delay enzyme dissociation and would be expected to lengthen the surface residence time. Because this condition was most similar to the conditions used in our kinetic assays, we used the k_s value measured for the condition with ATP in our kinetic simulations (0.30 s^{-1} = 18 min^{-1}).

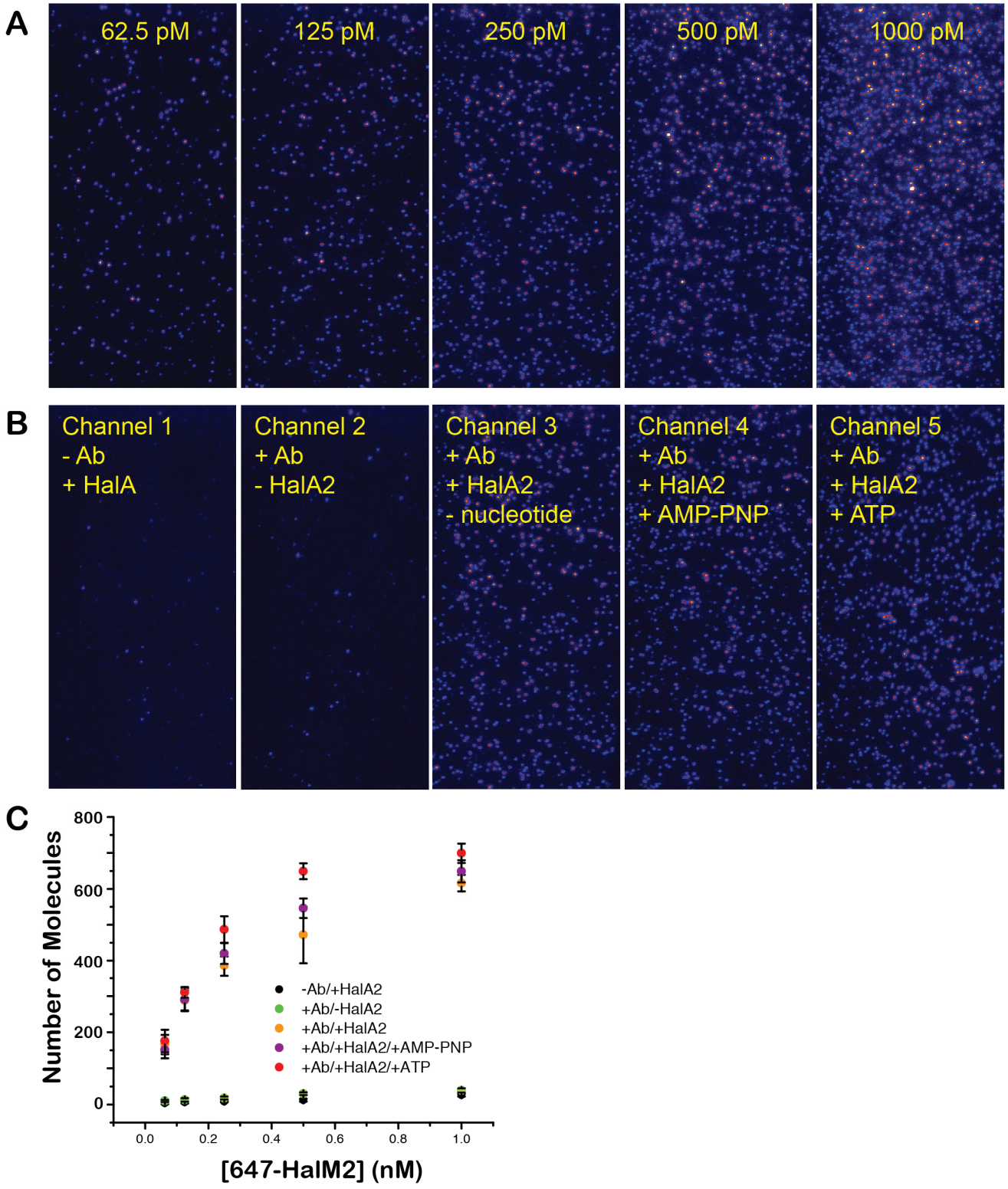

Figure S9. Single molecule binding assays for 647-HalM2. A) The dependence of the number of 647-HalM2 binding events on the solution concentration of 647-HalM2 (indicated in each panel). The surface in these panels is coated with His_6P-HalA2. **B**) Images showing that 647-HalM2 (250 pM) only binds to the surface in the presence of both anti His_6-Ab and His_6P-HalA2. **C**) The 647-HalM2 surface binding events from the images in **B** were detected and quantified by IDL and Matlab software and are plotted as a function of [647-HalM2].

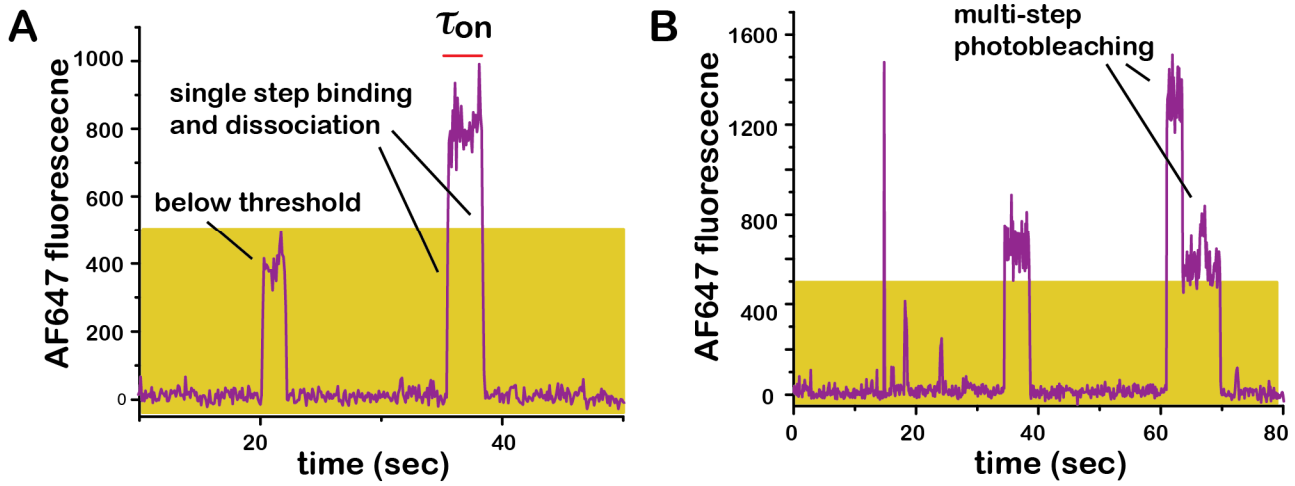

Figure S10. Representative single molecule binding events. Panels **A** and **B** show time-dependent fluorescence trajectories for two separate regions of a PEG surface coated with His_6P-HalA2 and incubated with 125 pM 647-HalM2 in the absence of ATP. Transient 647-HalM2 binding events are characterized by a binding time, τ_{on}, that reflects the HalM2:His_6P-HalA2 dissociation rate: $k_{off} = 1/\tau_{on}$.

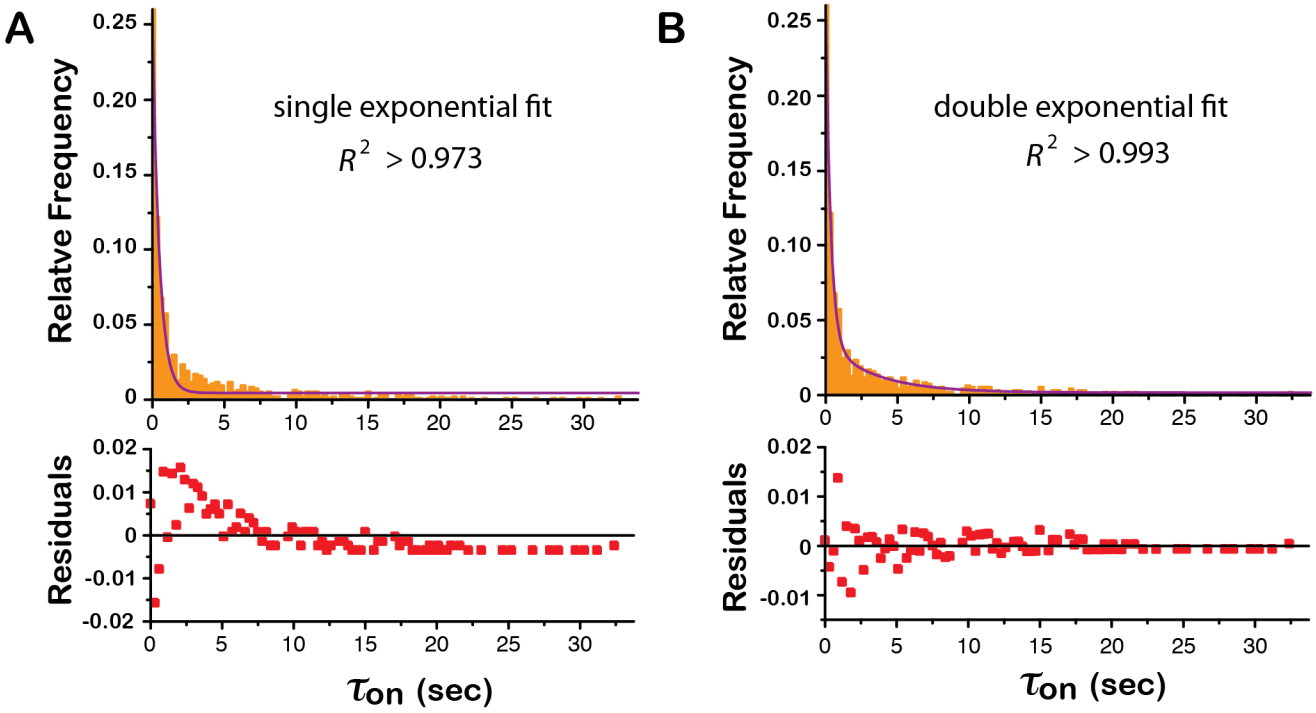

Figure S11. Estimating the ensemble HalM2:His_6P-HalA2 dissociation rate from single molecule binding events. From the τ_{on} values measured for single molecules as in Figure S10, ensemble histograms were constructed and fitted with exponential functions for the estimation of the rates of dissociation of 647-HalM2 from the surface. For all conditions analyzed, the ensemble τ_{on} distribution data was fit better with a double exponential function (right panels), indicating that two kinetically relevant dissociation processes contribute to the observed distribution of τ_{on}. The data shown are taken from the condition with His_6P-HalA2 immobilized on the surface and with 125 pM 647-HalM2 in the presence of 5 mM ATP. Parameter estimates for the different experimental conditions are listed in Table S4.

Table S4. Summary of single molecule binding data

		Parameter Estimates*			
		Fast Phase		Slow Phase	
condition	N	A_f	k_f (s^{-1})	A_s	k_s (s^{-1})
no nucleotide	999	0.40 ± 0.04	1.7 ± 0.36	0.07 ± 0.04	0.4 ± 0.2
+ AMP-PNP	1043	0.18 ± 0.01	2.7 ± 0.2	0.07 ± 0.01	0.5 ± 0.07
+ ATP	946	0.23 ± 0.004	2.9 ± 0.11	0.033 ± 0.004	0.30 ± 0.04**

* All data were fit with a double exponential equation: $y = A_f e^{-k_f t} + A_s e^{-k_s t} + C$

** This value for k_s was used in the kinetic simulations

N = number of binding events analyzed.

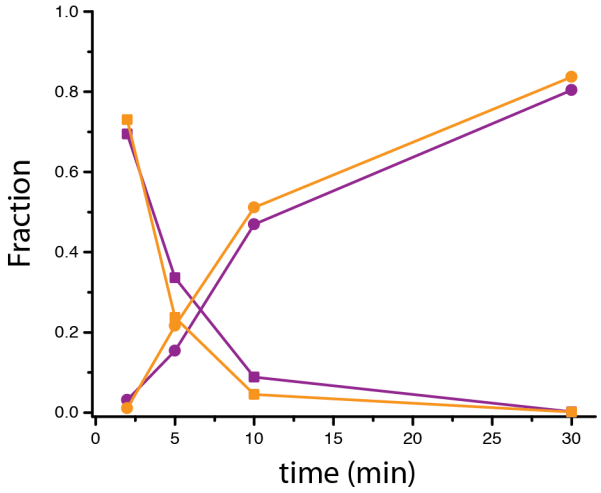

Figure S12. Effect of ATP concentration on HalM2/His_6P-HalA2 reaction kinetics. HalM2/His_6P-HalA2 kinetic assays were conducted at either 500 μM (purple) or 5 mM (orange) ATP under the otherwise standard reaction conditions described in the Methods section. Kinetic time courses are plotted for the starting material (**7**, [M+4NEM], squares) and the final product (**4**, [M+4Lan+3Dhx], circles). Fractional abundances for these species were calculated as described in the Methods section.

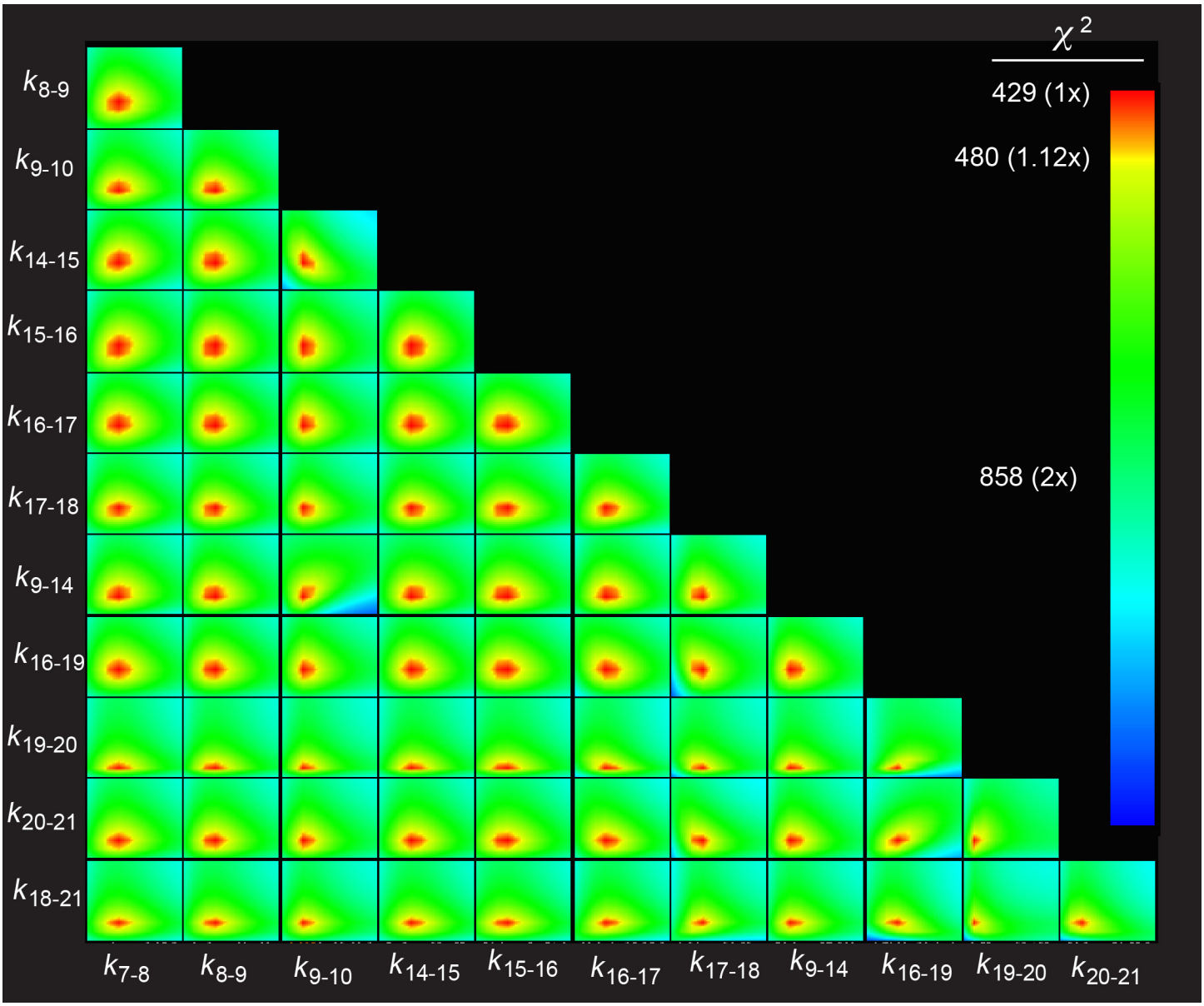

Figure S13. Estimating parameter boundaries in the HalM2/His$_6$P-HalA2 kinetic model with FitSpace Explorer. The kinetic data shown in Figure 4 of the main text were simulated with the kinetic model given in Scheme 3. Fitting of the data with the set of rate constants given in Table 1 yielded a χ^2 minimum of 429 (χ^2/DoF = 1.187). FitSpace Explorer was used to show that a χ^2 value within 1.12 times the χ^2 minimum (the red and orange regions in the plots above) could only be found for certain fixed values of each pairwise combination of each variable parameter. Thus, the magnitude for each variable parameter is well-constrained by the data. The χ^2 threshold of 1.12 times the χ^2 minimum provides a larger boundary range for the parameter estimates than the threshold suggested by FitSpace Explorer (1.06x).

Description of additional kinetic models for the HalM2/His_6P-HalA2 reaction: The HalM2/His_6P-HalA2 kinetic data were fit to several additional kinetic models (Scheme S1) in order to explore other potential features of the HalM2-catalyzed maturation of His_6P-HalA2. Here, for ease of discussion, we introduce a simple system for intermediate nomenclature where the compound numbers shown elsewhere in the text are replaced with a pair of numbers in brackets. The first number denotes the number of thioether rings in the compound and the second number denotes the total number of dehydrated Ser/Thr residues.

Model 1 corresponds to the model presented in the main text (Scheme 3, Figure 4, Table 1) and was used as the starting point for simulation of the additional models shown in Scheme S1 (models 2-6). Model 2 is a slight alteration of model 1, differing only in how the rate constants were linked during fitting. In model 2, the rate constants for each of the three cyclization steps leading to ring B formation ([1,4]→[2,4], [1,5]→[2,5], and [1,6]→[2,6]) as well as each of the three dehydration steps occurring on twice cyclized peptides ([2,4]→[2,5], [2,5]→[2,6], and [2,6]→[2,7]) were held at fixed relative ratios. Linking the rate constants in this altered arrangement yielded a slight improvement in the overall fit relative to model 1 with very little change in the magnitudes or FitSpace boundaries of the other variable parameters (Table S5). Even though there was a slight improvement in the fit to model 2, the magnitudes of the rate constants for the [1,6]→[2,6] and [2,4]→[2,5] reactions were individually well constrained in model 1, so we opted to present model 1 in the main text as this model contains an additional, well-constrained variable parameter.

Model 3 is a simplified version of model 1, where the cyclization reaction [1,5]→[2,5] is omitted. The impetus for testing this model was that we noticed that the two cyclization reactions [1,4]→[2,4] and [1,5]→[2,5] were not individually well-constrained. These steps appeared to represent minor pathways for the overall conversion of [1,4]→→[2,6], with the majority of the second cyclization occurring from intermediate [1,6]. When [1,5]→[2,5] was omitted, there was a slight change in some of the rates of the nearby steps in the mechanism ([1,4]→[2,4] and [2,4]→[2,5]) that reflect slightly altered flux from [1,4]→→[2,6]. This simplified mechanism gave a comparable, though slightly larger value for χ^2/DoF (Table S5), indicating that is it probably a valid model for the available kinetic data. However, it is difficult to provide a physical model for why the second cyclization would be able to proceed from [1,4] and [1,6], but not from [1,5]. Because of this, we concluded that model 1 was likely a more realistic depiction of the kinetic mechanism than model 3.

We also attempted to account for the His_6P-HalA2 species containing 3 thioether rings ([3,6] and [3,7], Scheme S1, model 4) that were observed at low abundance in the reaction spectra (**23** and **24**, respectively, Figure 1), but that were difficult to simulate with model 1. Inclusion of these species in the kinetic model required the replacement of the net rate [2,7]→[4,7] with four steps: [2,6]→[3,6], [2,7]→[3,7], [3,6]→[3,7], and [3,7]→[4,7]. Using the best fit rate constants from model 1 as a starting point, it was particularly difficult to accurately reconstruct the decay phase of the [3,6] and [3,7] intermediates, and the best fit we could obtain (using the same set of assumptions discussed in the main text,) had a significantly larger χ^2/DoF than the other models tested (Table S5, model 4b). However, we found that if we reduced the bimolecular binding rate of intermediates [3,6] and [3,7] approximately 15 fold from 10 $\mu M^{-1}min^{-1}$ to 0.73 $\mu M^{-1}min^{-1}$ (model 4), then we

could simulate the data with a reasonable set of rate constants. The simulated kinetic time courses for species [3,6] and [3,7] (Figure S14) show that reduction in the binding rate of these species significantly improves the simulation of their decay kinetics. Perhaps if released from the enzyme, these late stage intermediates are not as efficiently rebound and processed by HalM2 as other intermediates in the pathway, which may help prevent product inhibition.

To investigate the potential effects of having non-uniform binding kinetics, we simulated two additional variations of model 1 (models 5 and 6, Scheme S1). In both models, we assumed that the His_6P-HalA2 binding kinetics would be a function of the number of thioether rings in the peptide. In model 5, the K_d for all intermediates was held fixed at 1.8 μM, but the absolute magnitudes of k_{on} and k_{off} were allowed to vary for each group of intermediates (no thioether rings, one thioether ring, etc.). In model 6, both k_{on} and k_{off} for each group of intermediates were allowed to vary independently. After simulating the data under these conditions, the optimized binding and dissociation constants were once again fixed and the data were re-fit to give the parameter estimates shown in Table S5. As can be seen from Scheme S1 and the data in Table S5, modest changes in the values of the binding affinities can significantly alter the quality of the fit. This likely reflects the fact that the steady state concentrations of most HalM2/His_6P-HalA2 reaction intermediates remain low and comparable in magnitude to the K_d throughout the reaction (Table 1). In this scenario, binding kinetics will contribute significantly to the observed rate. One intriguing finding from the simulation of model 6 is that the binding affinity of HalM2 for intermediates seems to weaken as the intermediates become more highly modified (Scheme S1). Again, this could help to ensure efficient conversion of starting material to final product while minimizing extensive product inhibition. At present, we have not measured binding affinities for any of the HalA2 reaction intermediates. Thus, we have conservatively opted to present model 1 (which assumes identical binding peptide affinities) in the main text. Additional experiments will be helpful in refining the HalM2/His_6P-HalA2 kinetic model. *Importantly, these alternative models produced sets of rate constants that were very similar to those given by the model discussed in the main text (Table S5).*

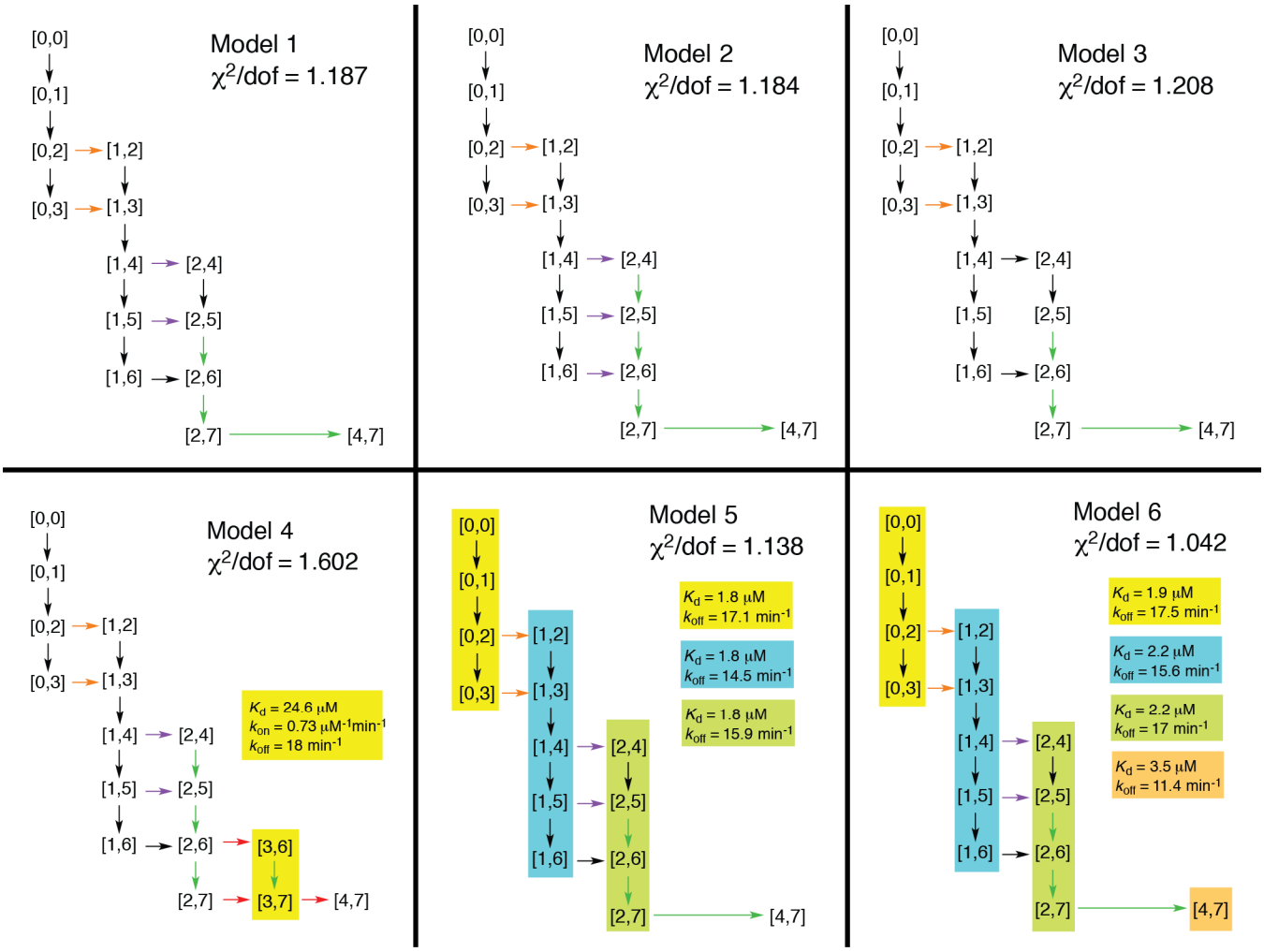

Scheme S1. Additional kinetic models for HalM2. The compound numbers used in the text are replaced here with an identifier that denotes the number of thioether rings and the total number of dehydrations (the first and second numbers in the square brackets, respectively) in order to facilitate depiction of the flow of intermediates from the starting material [0,0] to the final product [4,7]. Unless otherwise indicated, a fixed K_d and k_{off} (1.8 μM and 18 min^{-1}, respectively) was used for each intermediate during simulation. The colors of the arrows connecting the various species indicate how the rate constants were linked during non-linear fitting of the model to the data. Black arrows indicate rate constants that were allowed to freely vary. The reduced chi-square (χ^2/DoF) for each model is indicated. Rate constants for each model are listed in Table S5.

Table S5. Summary of simulated rate constants for additional HalM2/His_6P-HalA2 mechanisms depicted in Scheme S1. The K_d, k_{on}, and k_{off} values used are given in Scheme S1. Colors indicate which rate constants were linked during fitting. Black numbers were allowed to freely vary during fitting. All rate constants are in units of min^{-1}. FitSpace boundaries for parameter estimates (shown in parentheses in units of min^{-1}) are given at 1.12 times the χ^2 minimum of the fit.

Reaction	Model 1	Model 2	Model 3	Model 4b	Model 4	Model 5	Model 6
[0,0]→[0,1]	17 (15-19)	17 (16-19)	17 (16-19)	16	17 (16.5-19)	20 (20-24)	17 (16-19)
[0,1]→[0,2]	61 (57-70)	61 (61-70)	61 (61-70)	61	61 (61-67)	63 (63-72)	60 (56-66)
[0,2]→[0,3]	25 (16-38)	25 (16-31)	25 (16-38)	24	25 (13-38)	25 (16-39)	24 (15-30)
[0,2]→[1,2]	104 (91-117)	104 (91-117)	104 (91-117)	103	104 (101-130)	107 (104-117)	102 (100-112)
[0,3]→[1,3]	104	104	104	103	104	107	102
[1,2]→[1,3]	81 (70-89)	81 (73-89)	81 (72-89)	81	81 (75-89)	79 (71-87)	83 (77-93)
[1,3]→[1,4]	36 (33-40)	36 (34-40)	36 (33-40)	36	36 (34-41)	36 (33-39)	37 (35-40)
[1,4]→[1,5]	16 (14-18)	16 (15-18)	14 (13-15)	16	16 (16-19)	16 (14-17)	16 (14-18)
[1,5]→[1,6]	23 (19-29)	23 (19-29)	24 (19-29)	25	24 (19-30)	22 (18-28)	23 (18-28)
[1,4]→[2,4]	2.5 (1.9-3.2)	2.5 (2.3-2.8)	4.8 (3.7-6.0)	1.9	2.4 (1.9-3.0)	2.4 (1.9-3.0)	2.4 (1.9-3.0)
[1,5]→[2,5]	5.0	5.0	NA	3.7	4.8	4.8	4.8
[1,6]→[2,6]	20 (16-25)	20	21 (16-26)	22	21 (17-26)	19 (16-25)	19 (16-24)
[2,4]→[2,5]	19 (12-29)	19 (18-22)	40 (25-62)	13	18 (16-20)	18 (12-28)	19 (12-29)
[2,5]→[2,6]	32 (27-40)	32	31 (28-19)	22	31	31 (27-38)	31 (30-39)
[2,6]→[2,7]	58	58	58	40	56	57	58
[2,6]→[3,6]	NA	NA	NA	12	5.4 (4.4-6.8)	NA	NA
[2,7]→[3,7]	NA	NA	NA	33	39	NA	NA
[3,6]→[3,7]	NA	NA	NA	51	71	NA	NA
[3,7]→[4,7]	NA	NA	NA	88	290	NA	NA
[2,7]→→[4,7]	41	41	41	NA	NA	40	41
χ^2/DoF	1.187	1.184	1.208	3.176	1.602	1.138	1.042

NA – not applicable

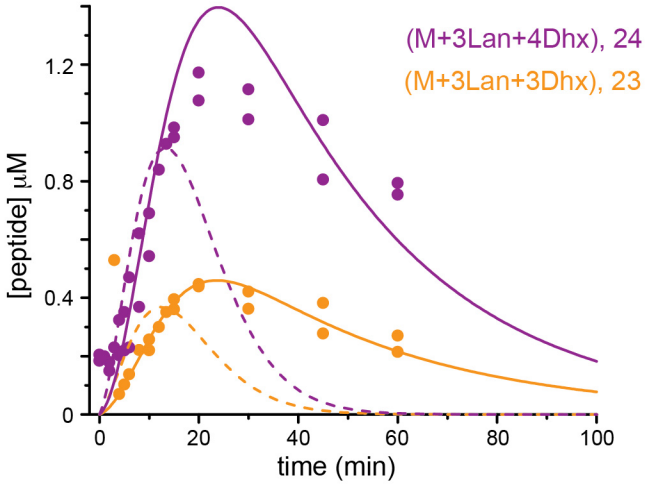

Figure S14. Kinetics of the His_6P-HalA2 reaction intermediates containing 3 thioether rings. Time courses for HalM2/His_6P-HalA2 reaction intermediates containing three thioether rings were simulated according to model 4 or 4b (Scheme S1, Table S5). In these models, the binding kinetics for species **23** and **24** were either held fixed and equivalent to the binding kinetics for the other reaction intermediates (model 4b, dashed lines), or k_{on} was allowed to vary at fixed k_{off} (model 4, solid lines). The reduction in k_{on} in model 4 (from 10 $\mu M^{-1}min^{-1}$ to 0.73 $\mu M^{-1}min^{-1}$) leads to better simulation of the observed decay kinetics for these species.

IV. Additional Experiments Related to the Kinetic Characterization of ProcM

Determining the ProcM/ProcA2.8 binding affinity: We attempted to measure the ProcM/ProcA2.8 dissociation rate (k_{off}) using the single molecule binding assay described above for HalM2, but we had difficulties measuring specific binding of ProcM to the imaging surface (data not shown). Instead, we measured the binding affinity (K_d) using a fluorescence polarization assay. In the assay, we site specifically labeled ProcA2.8 on the *N*-terminus using the aldehyde tag strategy developed by Bertozzi (Scheme S2).[10,11] Below, we describe methods for the preparation of the aldehyde-tagged ProcA2.8 construct, as well as conditions for the *in vitro* formylglycine generating enzyme (FGE)-mediated modification of the tag, validation of FGE activity, and fluorescent labeling of the aldehyde-tagged peptide with a hydrazide conjugate.

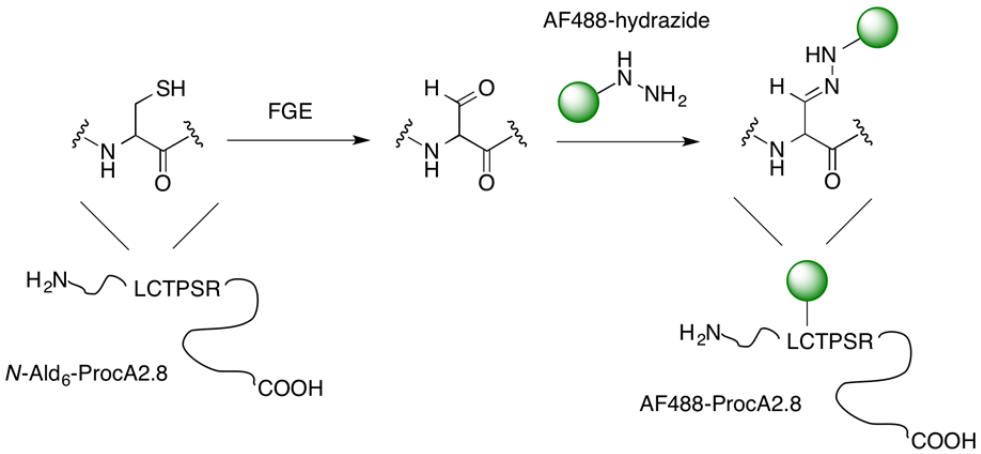

Scheme S2. Aldehyde tag strategy for site-specific labeling of ProcA2.8.

Constructing an expression vector to introduce an N-terminal aldehyde tag onto ProcA2.8: For the fluorescence polarization binding experiments discussed below, we constructed a site-specifically labeled ProcA2.8 construct. Our strategy involved genetically fusing an aldehyde tag to the *N*-terminus of ProcA2.8. We first mutagenized the pET28 vector to contain an aldehyde tag sequence (LCTPSR) on the 5′ side of the Nde1 restriction site. The sequence of the mutagenesis primers were: 5′-GTGCCGCGCGGCAGCCTGTGCACCCCGAGCCGCATATGGCTAGCATG and its reverse complement. The underlined sequence encodes for the LCTPSR aldehyde tag. The insertion was introduced into pET28 using the QuikChange Lightning mutagenesis kit (Agilent). The PCR reaction contained 50 ng vector (pET28) and 0.5 μM of each primer. All other PCR reaction components, the PCR cycling conditions, digestion of parental DNA with DpnI, and the transformation of the mutagenized construct into *E. coli* XL10-Gold were carried out as suggested by the manufacturer. The plasmid (dubbed *N*-Ald_6-pET28) was then propagated in and recovered from *E. coli* XL10 and sequenced to verify the presence of the aldehyde tag insertion. The *procA2.8* gene was then amplified with standard techniques from the ProcA2.8/pET15 vector described previously[3] using the following PCR primers: forward: 5′-GGGAATTCCATATGTCAGAAGAGCAACTG and reverse: 5′-CCGCTCGAGTTAGCACTCACCCTC. The PCR product was then cloned into the NdeI/XhoI sites of the *N*-Ald_6-pET28 vector using standard molecular biology techniques to construct the *N*-Ald_6-ProcA2.8/pET28 construct. The sequence of this construct was verified and *E. coli* BL21(DE3) cells were transformed with the plasmid. The *N*-Ald_6-ProcA2.8 peptide was then expressed and purified in a manner very similar to that described in the *Preparation of LanA peptides* section.

Expression and Purification of the Formylglycine Generating Enzyme (FGE): The *fge* gene from *Mycobacterium tuberculosis* in the pBAD/c-myc HisA vector (Addgene) was PCR amplified and cloned into the NdeI/XhoI sites of pET28. The FGE/pET28 construct was transformed into *E. coli* BL21 (DE3), and the His_6-tagged FGE enzyme was expressed and purified as described by Bertozzi and co-workers.[10]

In vitro FGE modification of N-Ald_6-ProcA2.8: Following conditions similar to those used by Bertozzi and co-workers,[11] we set up an *in vitro* FGE modification reaction containing 200 μM *N*-Ald_6-ProcA2.8, 62.5 μM FGE, 2 mM DTT, 0.2 mg/mL BSA, 68 mM NaCl, and 50 mM Tris (pH 9.0). The reaction was incubated for 2 h at 30 °C at which point 10 μL of 10% TFA was added to quench the reaction. The reaction was centrifuged to remove the precipitate and the peptide present in the supernatant was purified by C4-SPE as described above. To verify that FGE indeed oxidized the Cys residue in the aldehyde tag (LCTPSR) of *N*-Ald_6-ProcA2.8 into a formylglycine residue (FGly), the eluate from the C4-SPE column (containing *N*-Ald_6-ProcA2.8) was treated with 2,4-dinitrophenylhydrazine (DNP, Sigma). For this assay, we set up a 1 mL reaction containing approximately 4 μM of *N*-Ald_6-ProcA2.8 (100 μL from the 1 mL C4-SPE eluate), 15.7 mM DNP, and 0.5% TFA in 87% MeCN. We also set up a control reaction lacking DNP. These samples were reacted at 37 °C for 3 days, flash frozen, lyophilized, resuspended in H_2O and centrifuged. The supernatant was purified by C4-SPE

a second time, lyophilized, resuspended in buffer and digested with LysC as described above. The digested samples were purified with a C18 zip tip (Millipore) and analyzed by MALDI-TOF-MS using a saturated α-cyano-4-hydroxycinnamic acid solution (TCI Chemicals) in 80% MeCN, 0.1% TFA as the matrix. In the sample that was not treated with DNP (Figure S15A), there appeared to be very efficient FGE-mediated conversion of the Cys residue in the LCTRSP sequence to an FGly residue ($[M+H]^{1+}_{avg,calc}$= 3537, $[M+H]^{1+}_{avg,obs}$= 3538). Upon DNP treatment, this peak was consumed and a new peak corresponding to the DNP adduct of the FGly-containing *N*-Ald$_6$-ProcA2.8 peptide appeared (Figure S15B, $[M+H]^{1+}_{avg,calc}$ = 3717, $[M+H]^{1+}_{avg,obs}$ = 3717). These data strongly suggested the *in vitro* FGE modification was efficient under our conditions.

Site-specific labeling of N-FGly-ProcA2.8: The FGE-treated *N*-Ald$_6$-ProcA2.8 peptide (140 μM) was then reacted with AlexaFluor 488 hydrazide (AF488, Life Technologies) in 75% MeCN, 0.5% TFA for 3 h at 37 °C. The sample was lyophilized, redissolved in 200 μL of H_2O, and purified by C4-SPE to remove the unreacted AF488. The C4-SPE eluate was mixed 1:1 with a saturated solution of α-cyano-4-hydroxycinnamic acid matrix (in 80% MeCN) and was analyzed by MALDI-TOF-MS (Figure S15C). The mass spectrum shows partial labeling of FGE-treated *N*-Ald$_6$-ProcA2.8 ($[M+H]^{1+}_{avg,calc}$ = 11561; $[M+H]^{1+}_{avg,obs}$= 11546) with AF488 to give AF488-ProcA2.8 ($[M+H]^{1+}_{avg,calc}$= 12113; $[M+H]^{1+}_{avg,obs}$= 12104). The labeling efficiency was calculated by UV-visible absorption spectroscopy to be 38%.

Fluorescence polarization assay to measure the ProcM:ProcA2.8 binding affinity: To determine the ProcM/ProcA2.8 binding affinity, the AF488-ProcA2.8 peptide was incubated with variable concentrations of ProcM and the change in fluorescence polarization was measured. Assays contained 20 nM AF488-ProcA2.8 (53 nM total ProcA2.8, including the unlabeled peptide), variable [ProcM] ranging from 0.25 – 100 μM, 10 mM $MgCl_2$, 1 mM TCEP, 50 mM HEPES, 14.3 mM Tris, 85.7 mM NaCl, 2.86% glycerol, pH 7.5. The Tris, NaCl, and glycerol originated from the enzyme storage buffer. These reagents were maintained at constant concentration in all samples in order to minimize any effects they might have had on the fluorescence polarization signal. Triplicate samples were prepared for each concentration of ProcM analyzed. Each sample (100 μL) was transferred to its own well in a black-sided, glass bottom 96 well plate (Costar, product number 3615) and the plate was incubated at 27 °C for 1 h. Fluorescence polarization was measured with a Synergy H4 Hybrid Reader (BioTek) using 485/20 and 528/20 band-pass filters on the excitation and emission photons, respectively. The fluorescence intensities in the parallel and perpendicular directions ($F_{\parallel}$ and $F_{\perp}$, respectively) were corrected for scattering induced by the enzyme using a calibration curve derived from samples of varying concentration of ProcM on the same 96-well plate. These calibration curve samples lacked AF488-ProcA2.8, but were otherwise identical to samples described above. After correcting $F_{\parallel}$ and $F_{\perp}$ for scattering, the fluorescence polarization (mP) was calculated using Equation S1.

Equation S1.

$$mP = \left(\frac{F_{\parallel} - F_{\perp}}{F_{\parallel} + F_{\perp}}\right) \times 1000$$

The dependence of the polarization signal on the concentration of ProcM was then fitted with a hyperbola (Equation S2) to estimate the K_d for the ProcM/ProcA2.8 binding affinity (Figure S15D).

Equation S2.

$$mP = \left(\frac{max * E}{K_d + E}\right) + C$$

Here, max is the maximum polarization signal, E is the ProcM concentration, and C is an offset. Fitting of the data in this manner gave a K_d value of 4.7 μM, which was used in the kinetic simulations of the ProcM/ProcA2.8 reaction.

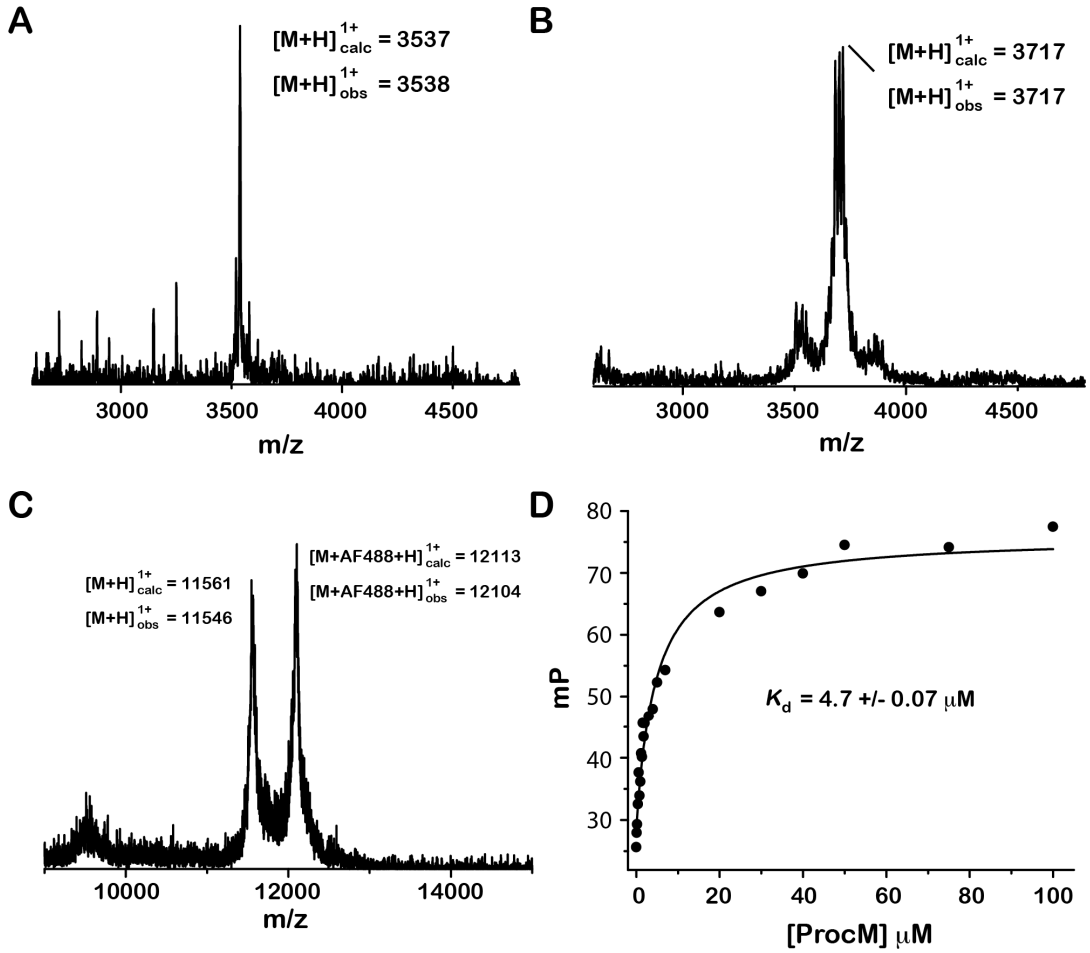

Figure S15. Measurement of the ProcM:ProcA2.8 binding constant with fluorescence polarization**.** A) MALDI-TOF mass spectrum of *N*-Ald$_6$-ProcA2.8 treated with FGE and digested with LysC. B) MALDI-TOF mass spectrum of *N*-Ald$_6$-ProcA2.8 treated with FGE and 2,4-dinitrophenylhydrazine and digested with LysC. C) MALDI-TOF mass spectrum of full length *N*-Ald$_6$-ProcA2.8 treated with FGE and subsequently reacted with AlexaFluor 488 hydrazide. Labeling is partial and the labeling efficiency was calculated to be 38% by UV-visible absorption spectroscopy. D) Fluorescence polarization titration of AF488-ProcA2.8 with ProcM.

Additional discussion and control experiments for the ProcM/ProcA2.8 reaction: An additional step (**26b** → **26**, Scheme 5) had to be included in the mechanism in order to account for the biphasic consumption of starting material (**26**). In this model, there is an inactive form of the substrate (**26b**) that must be converted to the active form (**26**) prior to ProcM-mediated processing. Non-linear fitting of the decay kinetics for species **26** clearly suggested that the consumption of **26** is biphasic and is characterized by fast and slow phases (Figure S16). The nearly equivalent amplitudes of the fast and slow phases (A_{fast} = 18 μM and A_{slow} = 20 μM), suggested that approximately half of the ProcA2.8 present at the start of the reaction was in the inactive form (**26b**). Because of this, the starting concentrations of **26** and **26b** were set to 20 μM in our simulations. The apparent rate for the slow phase (k_{slow} = 0.005 ± 0.0009 min^{-1}) was used to estimate the rate of conversion of the inactive form of the substrate to the active form ($k_{26b\rightarrow 26}$). This rate was held fixed during simulation of the model. The slow conversion of **26b** → **26** limits the reaction at later time points.

Species **26b** is likely an oxidized form of **26**, perhaps involving intermolecular or intramolecular disulfide bonds. Evidence for this claim was obtained when the TCEP concentration in the kinetic assay was increased from 0.1 to 1 mM. This alteration increased the fast phase amplitude to 90% of the total peptide (Figure S17A), suggesting that a larger portion of the ProcA2.8 substrate was in the active form at the start of the assay. However, the higher concentration of TCEP in the assay also led to a marked increase in the formation of TCEP adducts with reaction intermediates containing Dha residues (Figure S17B). These TCEP adducts were not completely consumed by ProcM during the assay (Figure S18). Changing the reducing agent from TCEP to DTT also resulted in adduct formation between the reductant and Dha residues (Figure S18). Because of these technical difficulties, the TCEP concentration in the kinetic assays was held to a minimum. We also considered whether TCEP adduct formation with species **29** to form species **40** could be responsible for the slow apparent cyclization kinetics of formation of ring A (**29** → **6**). However, during the majority of the reaction, species **40** represented only a minor fraction of species **29** (< 20%); thus, the majority of the substrate for the second cyclization was present in the appropriate form (i.e. as species **29**).

The phosphorylated species observed during the course of the reaction (**33**, **38**, and **39**) were not included in the kinetic model depicted in Scheme 5. These phosphorylated species were minor intermediates that accounted for a summed total of less than 8% of the total peptide at all time points in the reaction. We attempted to account for species **33** (M+Lan+P) and **39** (M+P) with the alternative model depicted in Scheme S3 (model 2). Compound **38** (M+P+Dha) was clearly detectable in the mass spectra (Fig. S4), but the time-dependent changes in the fractional abundance of this species could not clearly be distinguished from background signal. For this reason, we did not attempt to model kinetics for **38**. In model 2, we considered the phosphorylated species **33** and **39** to be intermediates along a minor reaction pathway (**26** → **39** → **33** → **29**, Scheme S3) that runs parallel to the major reaction pathway (**26** → **35** → **34** → **29** → **6**). The model was well fit with five variable rate constants, holding the $k_{34\rightarrow 35}/k_{33\rightarrow 29}$ and $k_{35\rightarrow 29}/k_{39\rightarrow 33}$ ratios constant (χ^2/DoF = 1.508, Fig. S19). In this model, the [M+P] species (**39**) is converted directly to the [M+Lan+P] species (**33**) in a single step ($k_{39\rightarrow 33}$ = 0.16 min^{-1}). Compound **38** may be an intermediate in this process (**39** → **38** → **33**). The

low-level accumulation of **38** could result if **38** is consumed to form species **33** faster than it is formed from species **39**.

The most intriguing feature of model 2 is that the rates of the chemical transformations along the minor pathway appear to be quite a bit slower than the other rates in the mechanism. For example, the net rate of formation of the first Lan ring ($k_{39\rightarrow33}$ = 0.16 min^{-1}) is significantly slower than the rate of formation of the first Lan ring along the major pathway ($k_{34\rightarrow29}$ = 2.1 min^{-1}). One possible physical explanation for this observation is that perhaps Ser9 (which is typically dehydrated 2nd by ProcM)[12] can be phosphorylated by ProcM prior to Ser13 dehydration at a low frequency (approximately 6% of the reaction flux partitions from **26** $\rightarrow$ **39**, Scheme S3). The untimely phosphorylation of Ser9 may perturb interactions between the ProcA2.8 core peptide and the dehydratase and/or cyclase active sites that are required for dehydration of Ser13 and the subsequent cyclization to from ring B. This could serve to lower the net rate for dehydration and cyclization at Ser13.

The rate of phosphate elimination from species **33** ($k_{33\rightarrow29}$ = 0.067 min^{-1}) is also much slower than both net dehydration rates in the major pathway ($k_{26\rightarrow35}$ = 1.4 min^{-1} and $k_{35\rightarrow34}$ = 13 min^{-1}). The sluggish phosphate elimination step ($k_{33\rightarrow29}$ = 0.067 min^{-1}), could be a result of the large molar excess of ATP (over ADP) in the assay, which is expected to inhibit formation of the active phosphopeptide:ADP:ProcM complex that is required for phosphate elimination.[13] In this scenario, the leader peptide of **33** binds to the enzyme with the same affinity as the other intermediates, but catalytically competent docking of the phosphopeptide into the dehydratase active site is inefficient because it requires ADP that is present in very low concentrations (it is formed in the dehydration process), and this effectively limits the net rate of conversion of species **33** $\rightarrow$ **29**. In line with this hypothesis, we could not detect phosphate elimination when the ProcA2.8-pS13 substrate (described in the "*Preparation of a phosphorylated ProcA2.8 derivative*" section) was incubated with ProcM under standard assay conditions (Figure S20). Instead, elimination was only observed in the presence of added ADP (Figure S20). Additional experiments should help to clarify this minor segment of the ProcM/ProcA2.8 reaction. It should be emphasized that the minor reaction pathway introduced into model 2 makes only slight contributions to product formation, and these preliminary simulations suggest that the majority of the reaction flux in this alternative model (94%) occurs via the route reported in Scheme 5 of the main text (i.e. **26** $\rightarrow$ **35** $\rightarrow$ **34** $\rightarrow$ **29** $\rightarrow$ **6**). Thus, the simplified kinetic model for the ProcM/ProcA2.8 reaction presented in Scheme 5 is likely a fairly accurate representation of the reaction pathway.

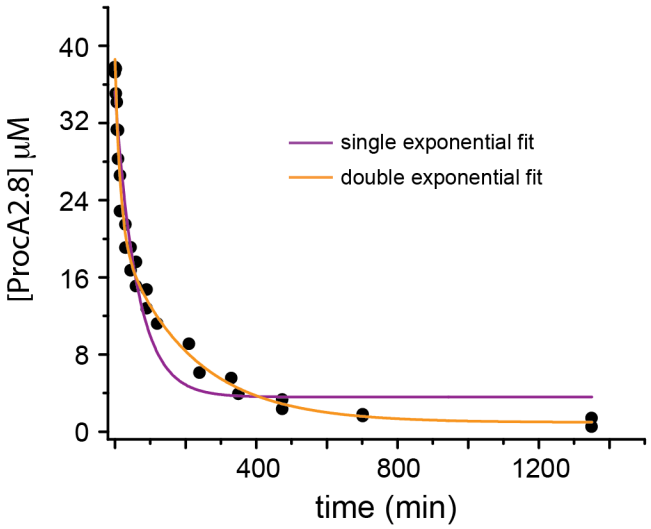

Figure S16. Biphasic consumption of ProcA2.8 starting material during the ProcM-catalyzed reaction. Kinetic data for species **26** were fit with either a single (purple) or double exponential equation (gold). The double exponential equation gave the best fit (R^2 > 0.99) and the following parameter estimates: A_{fast} = 18 ± 2 μM, k_{fast} = 0.7 ± 0.1 min^{-1}, A_{slow} = 20 ± 1.4 μM, k_{slow} = 0.005 ± 0.0009 min^{-1}. The slow phase rate (0.005 min^{-1}) was used as the rate of conversion of the inactive form of starting material to the active form (**26b** → **26**, Scheme 5).

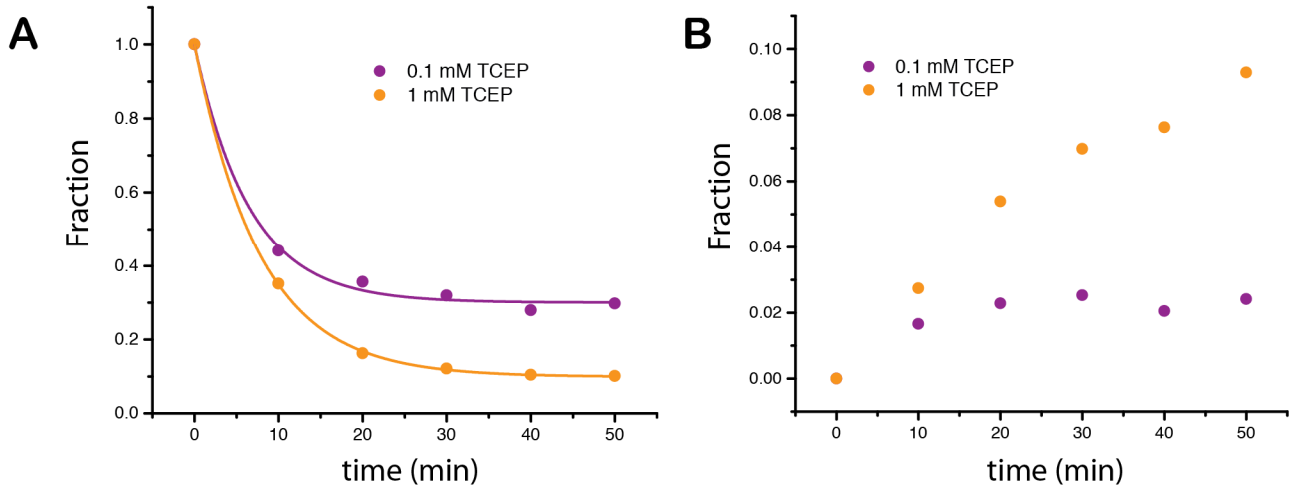

Figure S17. Effect of TCEP concentration on ProcM/ProcA2.8 reaction. **A**) ProcM-catalyzed consumption of the ProcA2.8 starting material (**26**) was measured in the presence of 0.1 or 1 mM TCEP under conditions that were otherwise identical to the standard kinetic assay described in the main text. Data were fit with a single exponential equation in order to estimate the rate and amplitude of the fast phase. For the 0.1 mM TCEP condition: A = 0.70 ± 0.02, k = 0.15 ± 0.02 min^{-1}. For the 1 mM TCEP condition: A = 0.90 ± 0.005, k = 0.128 ± 0.002 min^{-1}. **B**) In the same reaction, the amount of the TCEP adduct formed with 2-fold dehydrated ProcA2.8 species increased in the presence of 1 mM TCEP. Here, we plot the sum of species **40** and **41** - the signals for the TCEP adducts of species [M+Lan+Dha] (**29**) and [M+2Dha] (**34**), respectively.

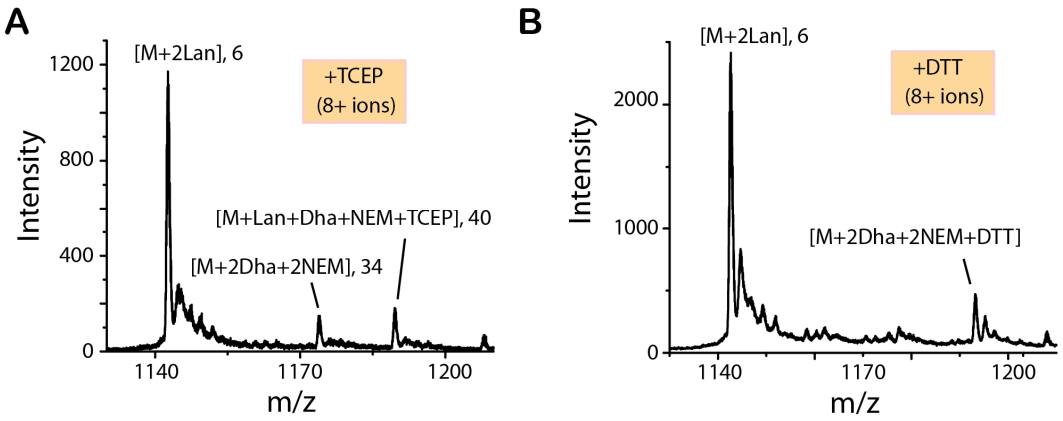

Figure S18. Adduct formation of ProcM/ProcA2.8 reaction intermediates and reducing agents. Reactions were incubated with 1 mM TCEP (panel A) or 1 mM DTT (panel B) for 24 h under standard reaction conditions and were analyzed with the same LC-ESI-MS conditions described for the ProcM/ProcA2.8 in the "*Assigning intermediates in the HalM2/His$_6$P-HalA2 and ProcM/ProcA2.8 reactions*" section of the Supporting Information. In both reactions, the expected final product (**6**) was the major species ($[M+H]_{obs}$ = 9129.432-*0*; $[M+H]_{calc}$ = 9129.310-*0*), but significant quantities of adducts between the reductant and dehydrated peptides were also present and were apparently not consumed during the reaction. In the reaction containing DTT, the major adduct was formed between DTT and compound **35**, the two-fold dehydrated ProcA2.8 intermediate ($[M+H]_{avg,obs}$ = 9533.293-*0*; $[M+H]_{calc}$ = 9533.417-*0*). In the reaction containing TCEP, the major TCEP adduct formed with compound **29** (the ProcA2.8 intermediate containing one Lan ring and one Dha residue) to give species **40** with mass: ($[M+H]_{obs}$ = 9504.291-*0*; $[M+H]_{calc}$ = 9504.418-*0*). The 8$^+$ peptide ions are shown.

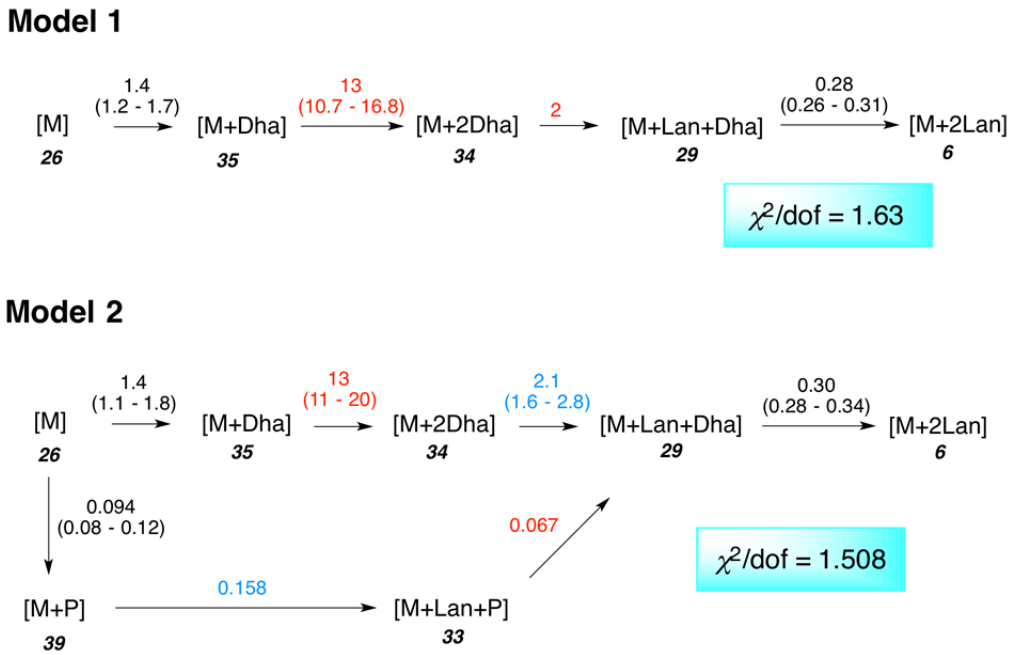

Scheme S3. Alternative kinetic model for the ProcM/ProcA2.8 reaction. The conversion of **26b** → **26** is not shown, but was included in both models ($k_{26b\rightarrow 26}$ = 0.005 min^{-1}). The binding and dissociation steps of the intermediates from the enzyme are also not depicted. These rates were held constant for all species (k_{on} = 4.25 μM^{-1}min^{-1} and k_{off} = 20 min^{-1}). The rate constants are in units of min^{-1} and are color coded according to how they were linked during non-linear regression. Rate constants in black were allowed to vary freely. FitSpace boundary estimates for rate constants (in units of min^{-1}) are shown in parentheses. Each species is numbered according to the assignments given for their corresponding NEM-alkylated derivatives in Figure S4 and Table S2. Model 1 is the model discussed in the main text. Model 2 is the alternative model taking into account observed phosphorylated peptides discussed in the Supporting Information.

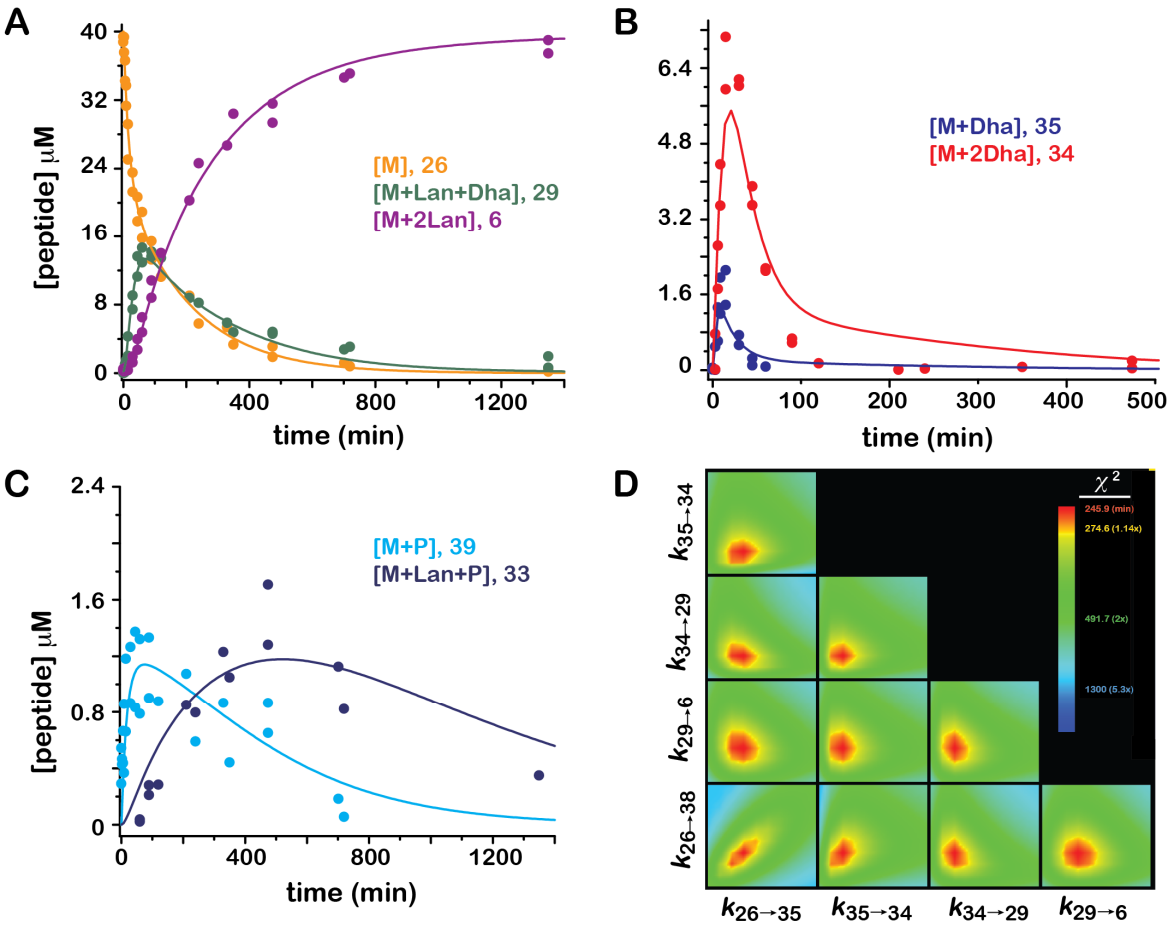

Figure S19. Simulation of ProcM/ProcA2.8 kinetic data with model 2 (Scheme S3). The overlay of data with simulated kinetic curves for the indicated species are shown in panels A-C. The FitSpace calculation for this model is shown in panel D. The parameter boundaries shown in Scheme S3 for this mechanism (the orange and red portions of the parameter space in panel D) are 1.14 times the χ^2 minimum of 245.9.

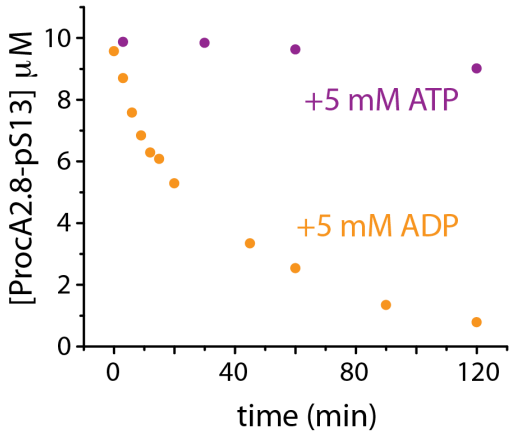

Figure S20. ADP is required for phosphate elimination in the ProcM/ProcA2.8-pS13 reaction. ProcM (1 μM) was incubated with 10 μM ProcA2.8-pS13 and 5 mM of either ATP or ADP under otherwise standard reaction conditions (see Methods section of main text). The conversion of ProcA2.8-pS13 to ProcA2.8-Dha13 was monitored using the standard LC-ESI-MS kinetic assay conditions given in the main text.

Table S6. Effect of the magnitude of k_{off} on the fitted parameter values for the rate constants in the ProcM/ProcA2.8 reaction. The $k_{35\rightarrow34}/k_{34\rightarrow29}$ ratio was held constant during fits. The data show that simulations of the mechanism in Scheme 5 with different fixed values of k_{off} result in similarly constrained values for the variable parameters in the model over a relatively broad range of k_{off} values

k_{off}	k_{on}*	K_d (μM)	$k_{26b\rightarrow26}$	$k_{26\rightarrow35}$	$k_{35\rightarrow34}$	$k_{34\rightarrow29}$	$k_{29\rightarrow6}$	χ^2/dof
2%	0.426	4.7	0.005	4.4	9.9	1.7	0.27	1.83
4	0.85	4.7	0.005	2.1	11.7	1.8	0.28	1.52
				(1.7 – 2.7)°	(9.4 – 14.7)		(0.25 – 0.32)	
10	2.13	4.7	0.005	1.53	12.9	1.9	0.28	1.53
				(1.2 – 1.9)	(10.3 – 16.1)		(0.26 – 0.32)	
20	4.26	4.7	0.005	1.38	13.4	2	0.28	1.63
				(1.2 – 1.5)	(10.8 – 16.8)		(0.26 – 0.31)	
50	10.6	4.7	0.005	1.29	13.8	2	0.29	1.73
				(1.1 – 1.4)	(11 – 17.2)		(0.27 – 0.31)	
100	21.3	4.7	0.005	1.27	13.9	2	0.29	1.77
				(1.1 – 1.4)	(11.1 – 17.3)		(0.27 – 0.31)	
200	42.6	4.7	0.005	1.23	14.2	2.1	0.29	1.79
				(1.1 – 1.4)	(11.4 – 17.8)		(0.27 – 0.34)	

%FitSpace boundaries were not calculated because the parameters were not well constrained by the mechanism shown in Scheme 5.

*k_{on} is in units of $\mu M^{-1}min^{-1}$. All other rate constants are in units of min^{-1}.

°All parameter boundaries are reported at 1.14 times the χ^2 minimum of the non-linear fit to the mechanism shown in Scheme 5.

Time dependent loss of ProcM activity.

Because of the slow kinetics of the ProcM-catalyzed reaction, we determined how fast ProcM activity was lost under our assay conditions. For these studies, ProcM was first diluted to 10 μM in assay buffer (5 mM $MgCl_2$, 0.1 mM TCEP, 100 mM HEPES, pH 7.5). This mixture was incubated at 25 °C and the activity of ProcM was then assayed at 0, 2, 4, 6, 8, and 23 h by diluting a portion of this mixture 10-fold into a freshly prepared reaction mixture containing the standard concentrations of reagents for ProcM/ProcA2.8 kinetic reactions given in the main text. After a 2 h incubation period, these reactions were quenched, NEM alkylated, C4-SPE purified and analyzed by LC-ESI-MS using the standard protocols reported in the main text. Time dependent changes in the fractional abundances of reaction intermediates were determined as described in the Methods section (Table S7). The data clearly show very little loss in ProcM activity within the first 8 h of the

preincubation. After 24 h, the only noticeable difference in ProcM activity is a slight reduction in the ability of the enzyme to catalyze the second cyclization reaction (the fraction of the [M+2Lan] intermediate decreases with a concomitant increase in the fraction of [M+Lan+Dha]). This observation suggests that the cyclase activity may be slightly more labile than the dehydratase activity. However, after 8 h (when ProcM activity is still maximal), the final product already accounts for approximately 75% of the total peptide (see the time courses in Figure 5). This observation suggests that ProcM activity loss under our conditions likely has only a marginal effect on the magnitude of the simulated rate constant for the second cyclization step ($k_{29\rightarrow6} = 0.28$ min^{-1}).

Table S7. Test for time-dependent loss of ProcM activity.

Length of preincubation	**Fractional Abundance (F_X)**						
(h)	[M+2Lan]	[M+Lan+Dha]*	[M+Lan+P]	[M+2Dha]	[M+Dha]	[M]	[M+P]
0	0.388805	0.216317	0.012533	0.026153	0.027241	0.314924	0.014028
2	0.365374	0.264744	0.012294	0.025426	0.01751	0.300157	0.014495
4	0.362072	0.259495	0.011368	0.022762	0.015564	0.313918	0.014821
6	0.391818	0.269409	0.010017	0.023315	0.013704	0.278236	0.013501
8	0.384754	0.27857	0.009803	0.024445	0.013367	0.275108	0.014853
23	0.264577	0.354196	0.007719	0.046437	0.013299	0.297901	0.015872

*The reported fractional abundance of [M+Lan+Dha] is the sum of the fractional abundance of two signals: the ion corresponding to [M+Lan+Dha+NEM], (species **29**) and the ion corresponding to its TCEP adduct, [M+Lan+Dha+NEM+TCEP] (species **40**).

References

(1) Johnson, K. A.; Simpson, Z. B.; Blom, T. *Anal. Biochem.* **2009**, *387*, 20.
(2) Johnson, K. A.; Simpson, Z. B.; Blom, T. *Anal. Biochem.* **2009**, *387*, 30.
(3) Li, B.; Sher, D.; Kelly, L.; Shi, Y.; Huang, K.; Knerr, P. J.; Joewono, I.; Rusch, D.; Chisholm, S. W.; van der Donk, W. A. *Proc. Natl. Acad. Sci. U.S.A.* **2010**, *107*, 10430.
(4) McClerren, A. L.; Cooper, L. E.; Quan, C.; Thomas, P. M.; Kelleher, N. L.; van der Donk, W. A. *Proc. Natl. Acad. Sci. U.S.A.* **2006**, *103*, 17243.
(5) Geoghegan, K. F.; Dixon, H. B. F.; Rosner, P. J.; Hoth, L. R.; Lanzetti, A. J.; Borzilleri, K. A.; Marr, E. S.; Pezzullo, L. H.; Martin, L. B.; LeMotte, P. K.; McColl, A. S.; Kamath, A. V.; Stroh, J. G. *Anal. Biochem.* **1999**, *267*, 169.
(6) Li, B.; Cooper, L. E.; van der Donk, W. A. *Methods Enzymol.* **2009**, *458*, 533.
(7) Thibodeaux, G. N.; van der Donk, W. A. *Chem Commun* **2012**, *48*, 10615.
(8) Dawson, P. E.; Muir, T. W.; Clark-Lewis, I.; Kent, S. B. *Science* **1994**, *266*, 776.
(9) Roy, R.; Hohng, S.; Ha, T. *Nat. Meth.* **2008**, *5*, 507.
(10) Carlson, B. L.; Ballister, E. R.; Skordalakes, E.; King, D. S.; Breidenbach, M. A.; Gilmore, S. A.; Berger, J. M.; Bertozzi, C. R. *J. Biol. Chem.* **2008**, *283*, 20117.
(11) Rush, J. S.; Bertozzi, C. R. *J. Am. Chem. Soc.* **2008**, *130*, 12240.
(12) Mukherjee, S.; van der Donk, W. A. *J. Am. Chem. Soc.* **2014**, *136*, 10450.
(13) Chatterjee, C.; Miller, L. M.; Leung, Y. L.; Xie, L.; Yi, M.; Kelleher, N. L.; van der Donk, W. A. *J. Am. Chem. Soc.* **2005**, *127*, 15332.